THE *SWIFT* BAT X-RAY SURVEY. III. X-RAY SPECTRA AND STATISTICAL PROPERTIES

M. AJELLO,[1] A. RAU,[2] J. GREINER,[1] G. KANBACH,[1] M. SALVATO,[2] A. W. STRONG,[1] S. D. BARTHELMY,[3]
N. GEHRELS,[3] C. B. MARKWARDT,[3] AND J. TUELLER[3]

ABSTRACT

In this concluding part of the series of three papers dedicated to the *Swift* BAT hard X-ray survey (BXS), we focus on the X-ray spectral analysis and statistical properties of the source sample. Using a dedicated method to extract time-averaged spectra of BAT sources, we show that Galactic sources have, generally, softer spectra than extragalactic objects and that Seyfert 2 galaxies are harder than Seyfert 1s. The averaged spectrum of all Seyfert galaxies is consistent with a power-law with a photon index of 2.00 ± 0.07. The cumulative flux-number relation for the extragalactic sources in the 14–170 keV band is best described by a power-law with a slope $\alpha = 1.55 \pm 0.20$ and a normalization of $9.6 \pm 1.9 \times 10^{-3}$ AGNs deg^{-2} (or 396 ± 80 AGNs all-sky) above a flux level of 2×10^{-11} ergs cm^{-2} s^{-1} ($\sim$0.85 mcrab). The integration of the cumulative flux per unit area indicates that BAT resolves 1%–2% of the X-ray background emission in the 14–170 keV band. A subsample of 24 extragalactic sources above the 4.5 σ detection limit is used to study the statistical properties of AGNs. This sample is composed of local Seyfert galaxies ($z = 0.026$, median value) and $\sim$10% blazars. We find that 55% of the Seyfert galaxies are absorbed by column densities of $N_{\rm H} > 10^{22}$ H atoms cm^{-2} but that none is genuinely bona fide Compton thick. This study shows the capabilities of BAT to probe the hard X-ray sky to the millicrab level.

Subject headings: galaxies: active — surveys — X-rays: binaries — X-rays: galaxies

Online material: color figures

1. INTRODUCTION

There is a general consensus that the cosmic X-ray background (CXB), discovered more than 40 years ago (Giacconi et al. 1962), is produced by integrated emission of active galactic nuclei (AGNs). Population synthesis models have successfully shown, in the context of the AGN unified theory (Antonucci 1993), that AGNs with various levels of obscuration and at different redshifts account for 80%–100% of the CXB below 4 keV (Comastri et al. 1995; Gilli et al. 2001; Treister & Urry 2005). Notwithstanding all the advances in the field, a major question remains: do Compton-thick sources exist in the numbers that seem to be required by population synthesis models (e.g., Comastri et al. 1995; Gilli et al. 2001) to reproduce the shape of the CXB emission? An indication of the existence of such a population comes from the analysis of the CXB fraction that is resolved into sources; Worsley et al. (2005) find that this fraction decreases with energy and that the unresolved component is consistent with being the emission of a yet undetected population of Compton-thick AGNs. In summary, much evidence points towards the existence of Compton-thick AGNs, while only a handful of them are known and studied.

The >10 keV energy range is the most appropriate band for studying and selecting an unbiased (with respect to absorption) sample of AGNs. This band is also the optimum band for the detection of Compton-thick objects. These elusive objects could have been missed because of the difficulties of performing sensitive imaging of the hard X-ray sky. The Burst Alert Telescope (BAT; Barthelmy et al. 2005), on board the *Swift* mission (Gehrels

et al. 2004), represents a major improvement in sensitivity for X-ray imaging of the hard X-ray sky. We refer readers to Ajello et al. (2007) for details about the BXS survey.

We applied an innovative image reconstruction algorithm to 8 months of survey BAT data; our survey covers $\sim$7000 deg^2, reaching a limiting sensitivity of <0.9 mcrab. This makes it one of the most sensitive surveys ever performed in the hard X-ray domain. We detected 49 hard X-ray sources, of which 37 were previously unknown as hard X-ray emitters. Correlation with X-ray catalogs allowed us to identify 15 sources, while pointed observations by *Swift* XRT provided identification for another 15 objects. Furthermore, we optically identified 3 new extragalactic sources (Rau et al. 2007). Here we investigate the spectral and statistical properties of all objects in the complete source sample.

The paper is organized as follows. In § 2 we present the X-ray spectral analysis of the BAT sources. The details of the dedicated spectral extraction method are presented in the Appendix. We use the source spectra to build an X-ray color-color plot, which is used to understand the mean properties of the source populations. In § 3 we apply the $V/V_{\rm max}$ method to test the completeness of the extragalactic sample, which is then used to derive the number-flux relation. The section ends with a discussion of the statistical properties of the extragalactic sample. Finally, we discuss the BAT results in § 4. Throughout this work we use $H_0 = 70$ km s^{-1} Mpc^{-1} ($h_{70} = 1$), $k = 0$, $\Omega_{\rm matter} = 0.3$, and $\Lambda_0 = 0.7$, and the luminosities are given in ergs s^{-1} h^{-1}.

2. SPECTRAL ANALYSIS

We have developed a dedicated spectral extraction method that allows to derive the time-averaged spectrum of all sources. The reader interested in the method is referred to the Appendix for details. Using this method, we derived for all our source candidates a six-channel energy spectrum in the range 14–195 keV. The energy channels used in this analysis are (in keV): 14–22,

[1] Max-Planck-Institut für extraterrestrische Physik, Postfach 1312, 85741, Garching, Germany.
[2] Caltech Optical Observatories, Mail Stop 105-24, California, Institute of Technology, Pasadena, CA 91125.
[3] Astroparticle Physics Laboratory, Mail Code 661, NASA Goddard Space Flight Center, Greenbelt, MD 20771.

TABLE 1
Spectral Parameters

Name	R.A. (J2000.0)	Decl. (J2000.0)	Type	$\Gamma/E[kT]$[a]	N_H (10^{22} atoms cm^{-2})	Model	Instrument[b]
3C 105.0	61.9178	3.6517	Seyfert 2	$1.66^{+0.13}_{-0.13}$	$29.4^{+5.7}_{-4.8}$	wabs*pow	B, X
1AXG J042556−5711	66.6021	−57.1775	Seyfert 1	$1.54^{+0.028}_{-0.027}$	0	pow	B, A
3C 120	68.2982	5.3374	Seyfert 1	$1.80^{+0.04}_{-0.04}/0.27^{+0.026}_{-0.025}$	0	wabs*pow+bb	B, A
MCG -01-13-025	72.9205	−3.8240	Seyfert 1.2	$1.6^{+0.48}_{-0.47}$	<0.02[c]	pow	B
SWIFT J0505.7−2348..................	76.4674	−23.8666	Seyfert 2	$1.77^{+0.08}_{-0.07}$	$4.8^{+0.9}_{-0.7}$	wabs*pow	B, X
CSV 6150	77.7224	16.5265	Seyfert 1.5	$1.94^{+0.25}_{-0.23}$	...	pow	B
4U 0513−40	78.5146	−40.0558	LXB	$29.7^{+7.5}_{-5.8}$	...	brem	B
QSO B0513−002	79.0096	−0.1332	Seyfert 1	$1.83^{+0.02}_{-0.016}/0.27^{+0.02}_{-0.02}$	< 0.01	wabs*pow+bb	B, A
SWIFT J0517.1+1633	79.2839	16.5605	...	$2.0^{+0.23}_{-0.26}$	...	pow	B
ESO 362− G 018	79.8844	−32.6720	Seyfert 1.5	$1.5^{+0.03}_{-0.02}$	<0.01	wabs*pow	B, X
Pictor A................................	79.9460	−45.7557	Seyfert 1	$1.8^{+0.015}_{-0.014}$	$0.12^{+0.007}_{-0.02}$	wabs*pow	B, A
ESO 362−G021	80.6581	−36.4233	BL Lac	$1.7^{+0.037}_{-0.036}$	$0.1^{+0.0197}_{-0.0187}$	wabs*pow	B, A, X
V* TV Col...............................	82.3541	−32.7965	CV−DQ*	$24.9^{+4.6}_{-3.8}$	...	bremss	B
V* TW Pic..............................	83.6470	−58.0200	CV	$13.5^{+10.6}_{-5.6}$	...	bremss	B
LMC X−3................................	84.7717	−64.1148	HXB	$2.0^{+0.4}_{-0.3}$	...	pow	B
LMC X−1................................	84.8917	−69.7210	HXB	$2.3^{+0.22}_{-0.20}$	...	pow	B
PSR B0540−69.3	84.9878	−69.3230	Pulsar	$1.85^{+0.28}_{-0.26}$	...	pow	B
PKS 0537−286..........................	84.9953	−28.7029	BLAZAR	$1.35^{+0.06}_{-0.08}$	< 0.01	wabs*pow	B, A
PKS 0548−322	87.7165	−32.2610	BL Lac	$1.8^{+0.032}_{-0.031}$	$0.02^{+0.006}_{-0.005}$	wabs*pow	B, X
NGC 2110...............................	88.0411	−7.4554	Seyfert 2	$1.62^{+0.01}_{-0.01}/0.47^{+0.02}_{-0.02}$	$4.0^{+0.13}_{-0.07}$	wabs*(pow+ga) + bb	B, A, X
LEDA 75476.............................	89.5237	−38.3799	Seyfert 1	$1.74^{+0.017}_{-0.025}/0.25^{+0.08}_{-0.05}$	$2.5^{+0.11}_{-0.17}$	wabs*(pow+ga)+bb	B, A
ESO 490− G 26	100.0031	−25.8931	Seyfert 1.2	$1.90^{+0.05}_{-0.04}$	$0.27^{+0.005}_{-0.005}$	wabs*pow	B, X
SWIFT J0727.5−2406..................	111.8951	−24.1039	...	$1.53^{+0.55}_{-0.54}$	...	pow	B
V* 441 Pup.............................	112.1626	−26.0696	CV	$12.4^{+13.6}_{-5.6}$	...	bremss	B
V* BG CMi	112.8752	9.9214	CV	$31.3^{+41.2}_{-14.2}$	...	bremss	B
SWIFT J0732.5−1331..................	113.1328	−13.5037	CV	$33.2^{+50.1}_{-14.2}$	...	bremss	B
SWIFT J0739.6−3144..................	114.9127	−31.7496	Seyfert 2[d]	$1.77^{+0.51}_{-0.43}$	>2[e]	pow	B
SWIFT J0743.0−2543..................	115.7501	−25.7314	...	$1.78^{+0.69}_{-0.56}$	...	pow	B
IGR J07597−3842......................	119.9822	−38.7422	Seyfert 1.2	$1.8^{+0.08}_{-0.07}$	<0.01	wabs*pow	B, X
UGC 4203................................	121.0552	5.1203	Seyfert 2	$1.68^{+0.09}_{-0.10}/0.31^{+0.08}_{-0.05}$	$12.5^{+5.0}_{-3.7}$[f]	wabs(pexrav+ga)+bb	B, A, X
SWIFT J0811.5+0937..................	122.8750	9.6214	XBONG[d]	$2.2^{+2.1}_{-0.9}$	0[g]	pow	B
SWIFT J0823.4−0457..................	125.8271	−4.9401	Seyfert 2	$1.84^{+0.28}_{-0.22}$	$19.3^{+6.8}_{-5.4}$	wabs*pow	B, X
Vela PSR	128.8308	−45.1771	PSR	$1.88^{+0.20}_{-0.26}$	...	pow	B
FRL 1146................................	129.6151	−35.9976	Seyfert 1	$1.88^{+0.37}_{-0.31}$	...	pow	B
3C 206	129.9556	−12.2467	QSO	$1.95^{+0.43}_{-0.39}$	0[g]	wabs*pow	B
SWFIT J0844.9−3531...........	131.2411	−35.5313	...	$1.91^{+0.46}_{-0.68}$	...	pow	B
SWIFT J0854.7+1502	133.6828	15.0371	Seyfert 2[d]	$1.41^{+0.7}_{-0.9}$	> 0.5[e]	pow	B
SWIFT J0917.2−6221................	139.112	−62.359	Seyfert 1	$1.87^{+0.07}_{-0.04}/0.14^{+0.02}_{-0.02}$	$1.33^{+0.18}_{-0.10}$	bb+wabs*pow	B
Mrk 0704..............................	139.6505	16.2987	Seyfert 1.5	$1.36^{+0.1}_{-0.07}$	$15.0^{+6.3}_{-3.5}$	pcfabs*(pow+ga)	B, A, X
4U 0919−54	140.0753	−55.2135	LXB	$45.11^{+26.13}_{-9.8}$	...	bremss	B
MCG -01-24-012	140.2134	−8.0872	Seyfert 2	$1.7^{+0.08}_{-0.07}$	$6.5^{+0.8}_{-0.7}$	wabs*pow	B, X
NGC 2992...............................	146.4060	−14.3007	Seyfert 1.9	$1.24^{+0.06}_{-0.06}$	$0.17^{-0.03}_{-0.03}$	wabs*(pow+ga)	B, A, X
ESO 434− G 040	146.9151	−30.9388	Seyfert 2	$1.77^{+0.006}_{-0.07}/0.15^{+0.011}_{-0.016}$	$1.5^{+0.026}_{-0.09}$	wabs*(pow+ga)+bb	B, A, X
3C 227	146.9447	7.4191	Seyfert 1	$2.11^{+0.14}_{-0.24}$	$3.6^{+1.5}_{-1.4}$	pexrav+wa*pow	B, C
NGC 3081...............................	149.8805	−22.8561	Seyfert 2	$1.9^{+0.02}_{-0.04}/0.58^{+0.15}_{-0.11}$	$60^{+3.1}_{-3.1}$	wabs*(pow+ga) +bb	B, A, S

[a] Photon index and/or plasma temperature for the model, specified in model column, to fit the data.
[b] Instruments used for spectral analysis are: B=BAT, X=*Swift* XRT, A=*ASCA*, C=*Chandra*, and S=*BeppoSAX*.
[c] Gallo et al. (2006).
[d] Proposed identification in Rau et al. (2007).
[e] Lower limit on absorption estimated through the nondetection by *ROSAT*.
[f] UGC 4203 exhibits transition between reflection- and transmission-dominated spectrum. The absorption is estimated in the latter case using XRT data (see text for details).
[g] Order of magnitude of the absorption estimated imposing that the extrapolated source flux match the *ROSAT* PSPC count rates.

22–30, 30–47, 47–71, 71-121, and 121–195. The energy bins were optimally chosen to produce similar error bars (in the different energy bins) for sources with power-law spectra. We found that 21 sources had at least soft X-ray observations by *Swift* XRT or *ASCA*. For these sources, we jointly fit XRT/*ASCA* and BAT data. When fitting a source spectrum, we have preferred the simplest model yielding a good description of the data. The normalization of the *ASCA* spectra was allowed to vary (with respect to the BAT ones) to cope with the different epochs of the observations. This was not required when fitting XRT and BAT data. In general, the BAT spectrum of Galactic sources is well fit by a thermal bremsstrahlung model. In contrast, AGNs are usually better described by a single power-law model. However, when <10 keV data were available, the fit required additional components (i.e., a blackbody component for soft excess and/or a Gaussian model for the iron line). The detailed analysis is reported in Appendix A4, while the spectral parameters are summarized in Table 1.
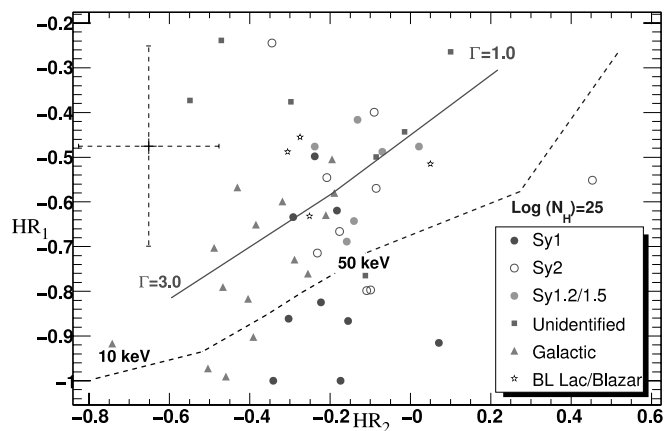
AJELLO ET AL.

Fig. 1.—Plot of HR1 and HR2 hardness ratios. The solid line is the locus for sources with unabsorbed power-law spectra with photon indices from 1.0 to 3.0, while the long-dashed line shows the location of Compton-thick AGNs with the same range of photon indices. The dashed line shows the location of objects with a thermal bremsstrahlung spectrum with temperatures in the range 5–50 keV. In the top left corner the typical $\pm 1\ \sigma$ error for a 5 σ source is shown. [*See the electronic edition of the Journal for a color version of this figure.*]

The properties of the source sample can be studied using hardness ratios. We have thus defined HR_1 and HR_2 as

$$HR_1 = \frac{medium - hard}{medium + hard},$$
$$HR_2 = \frac{soft - medium}{soft + medium}, \qquad (1)$$

where the *soft*, *medium*, and *hard* bands (in keV) are, respectively, 14–30, 30–71, and 71–195. The hardness ratios, shown in Figure 1, are normalized to the range −1 to +1. Different symbols indicate different source classes. We also indicate the loci occupied by sources with a power-law index in the range 1.0–3.0, or a bremsstrahlung spectrum with a temperature of 10–50 keV. A few things can be derived by the study of the hardness ratios. Galactic sources, usually characterized by soft X-ray spectra, have HR_2 values < -0.3 and $HR_1 < -0.5$, which is the typical region for sources with a steep photon index. Indeed, the five cataclysmic variables (CVs) present in the sample are all well fit by a relativistic bremsstrahlung model with a mean plasma temperature of 23 keV.

Similarly, we note that Seyfert 2 galaxies seem to have (given the large uncertainties) harder X-ray spectra than Seyfert 1s (larger values of HR_1). The fact that type 2 AGNs have systematically harder spectra than type 1 AGNs could be an evidence of the intrinsic difference between these two classes of objects. In order to study this issue in more detail, we performed a stacked spectral analysis[4] grouping the Seyfert galaxies detected by BAT into three classes: Seyfert 1, Seyfert 2, and intermediate Seyfert. The results, which are summarized in Table 2, show that the mean photon index of Seyfert 1s and Seyfert 2s are different at more than the 2 σ level. The same trend was previously noted in Seyfert galaxies detected by *OSSE* (Zdziarski et al. 2000) and by *INTEGRAL* (Beckmann et al. 2006). Zdziarski et al. (2000) find that the difference in spectral index could be due to the different viewing angle between Seyfert 1s and 2s. Indeed, the strength of Compton reflection decreases with the increasing viewing angle. Since the spectrum from Compton reflection peaks

[4] All stacked spectral analysis are performed doing a weighted average of the spectra.

TABLE 2
Spectral Parameters for Seyfert 1, Seyfert 2, Intermediate, and All Seyfert AGNs

CLASS	Photon Index	χ^2/NDF
Seyfert 1..	2.23 ± 0.11	5.4/4
Seyfert 2..	1.86 ± 0.10	1.2/4
Seyfert 1.2–1.5.............................	1.95 ± 0.11	4.9/4
Seyfert all......................................	2.00 ± 0.07	2.1/4

at 30 keV followed by a steep decline, the larger the reflection component, the softer the spectrum. We tested this scenario using for Seyfert 1s (Seyfert 2s are successfully fit by a simple power law) the `pexrav` (Magdziarz & Zdziarski 1995) model in XSPEC. Indeed, we get a good fit ($\chi^2 = 1.2/3$) with a (minimum) reflection strength $R > 1.1$ (upper limit is unconstrained by the fit), which is in good agreement with findings by Zdziarski et al. (2000) and Deluit & Courvoisier (2003). Thus, the BAT data seem to confirm the larger reflection component present in Seyfert 1 galaxies (with respect to Seyfert 2s), in agreement with the AGN unified model. Even though the reflection component improves the fit, it does not affect the photon index of Seyfert 1s, which remains 2.30 ± 0.12.

We note, however, that most of the Seyfert 1s (six out of nine) have a low value of HR_1, denoting a steep spectrum. We thus tried to fit the stacked spectrum with a cutoff power-law model of the form $E^{-\Gamma} e^{-(E/E_c)}$. Since the power-law index and the e-folding energy E_c are highly correlated, we fixed the photon index to 2.0 (see below). The best-fit e-folding energy is $110.8^{+68.4}_{-33.0}$ keV (90% CL), with a reduced χ^2 that is substantially better than the one of the power-law model (0.9 vs. 1.4, with an F-test probability of 0.08). The presence of a cutoff at $\sim$100 keV in the X-ray spectra of Seyfert 1s seems also to be confirmed by the analysis of Deluit & Courvoisier (2003).

Finally, we performed the stacked spectral analysis of all the Seyfert galaxies to investigate the averaged spectrum of the local AGNs detected by BAT. The stacked spectrum, shown in Figure 2, is consistent (in the 15–200 keV range) with a power-law model with a photon index of 2.00 ± 0.07 (90% CL).

3. THE HARD X-RAY EXTRAGALACTIC SAMPLE

The extragalactic sample, shown in Table 3, was derived from the catalog reported in Table 2 of Ajello et al. (2007), considering
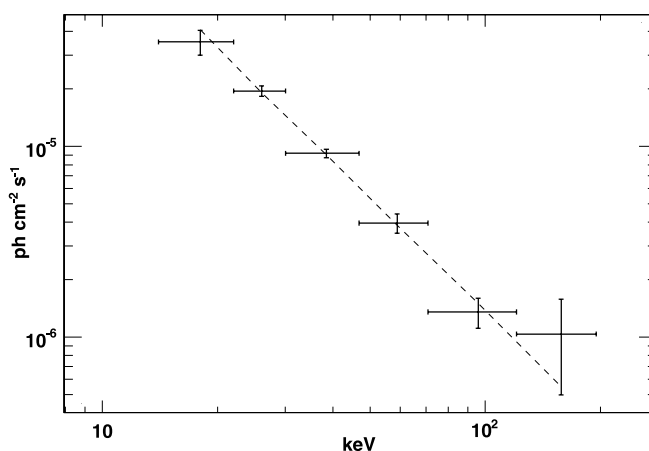

Fig. 2.—Stacked spectrum of all AGNs reported in Table 3 excluding the blazars. The dashed line is the best power-law fit to the data (photon index of 2.0 ± 0.07).

TABLE 3
EXTRAGALACTIC SAMPLE

Name	Type	z	Radio Loudness	Fx $(10^{-11}$ ergs cm^{-2} s$^{-1})$	Lx $(10^{43}$ ergs s$^{-1})$	$L_{2-10\,keV}/L_{O\,III}$[a]	Fe$_{EW}$[b] (eV)	N_H $(10^{22}$atoms cm$^{-2})$	References
3C 105.0	Seyfert 2	0.089	28421	$4.6^{+0.5}_{-0.4}$	44.5^{+17}_{-22}	581.5 ± 69.2	nr	29.4	1
1AXG J042556−5711	Seyfert 1	0.104	0.78[c]	$1.92^{+0.3}_{-0.2}$	55.0^{+10}_{-8}	...	nr	0	1
3C 120	Seyfert 1	0.0330	3762	$10.1^{+0.8}_{-1.8}$	$25.4^{+2.2}_{+4.5}$	148.8 ± 40.6	52.3	0	1
MCG -01-13-025	Seyfert 1.2	0.015894	1.15[c]	$2.52^{+1.1}_{-1.6}$	$1.5^{+0.6}_{-0.8}$	...	...	<0.02	2
SWIFT J0505.7−2348......	Seyfert 2	0.0350	7.13[c]	$5.0^{+0.7}_{-1.5}$	$14.1^{+0.24}_{-5.0}$	345.2 ± 82.2	nr	6.3	1
QSO B0513−002	Seyfert 1	0.0327	0.254	$4.92^{+0.9}_{-2.8}$	$12.3^{+2.1}_{-7.3}$	...	90.8	0.02	3
ESO 362− G 018.............	Seyfert 1.5	0.0126	0.58[c]	$5.0^{+0.7}_{-1.0}$	$1.7^{+0.3}_{-0.3}$	36.3 ± 3.7	nr	<0.01	1
Pictor A...........................	Seyfert 1	0.035	14045	$1.8^{+0.4}_{-1.2}$	$5.1^{+1.5}_{-3.7}$	113.4 ± 14.5	nr	0.12	1
ESO 362−G021................	BL Lac	0.05534	2409	$2.7^{+0.3}_{-0.3}$	$18.8^{+5.0}_{-0.5}$	1284.1 ± 270.3	nr	0.1	1
PKS 0537−286.................	BLAZAR	3.1	22000	$2.43^{+0.9}_{-3.0}$	$1.2^{+0.4}_{-0.4} \times 10^5$	...	nr	<0.01	1
PKS 0548−322.................	BL Lac	0.0690	383.33	$3.1^{+0.6}_{-1.0}$	$37.0^{+6.0}_{-11.0}$	...	nr	0.0257	1
NGC 2110........................	Seyfert 2	0.007789	26.92	$27.0^{+0.9}_{-1.0}$	$3.5^{+0.1}_{-0.1}$	1115.8 ± 101.4	118	4.0	1
LEDA 75476....................	Seyfert 1	0.0338	2.87[c]	$3.2^{+0.6}_{-1.2}$	$8.7^{+2.4}_{-2.1}$	393.7 ± 59.6	144	2.5	1
UGC 4203........................	Seyfert 2	0.01349	7.67	$4.28^{+0.6}_{-1.4}$	$1.7^{+0.3}_{-0.6}$	214.2 ± 71.4	747	12.5	1
SWIFT J0811.5+0937......	XBONG	0.282	268[c]	$1.55^{+1.2}_{-1.54}$	384^{+170}_{-200}	...	...	∼0[d]	
SWIFT J0823.4−0457......	Seyfert 2	0.023	0.61[c]	$2.78^{+1.0}_{-1.1}$	$3.3^{+1.1}_{-1.3}$	179.1 ± 71.6	...	16.2	1
3C 206	QSO	0.1976	1194	$2.62^{+0.7}_{-1.3}$	300^{+75}_{-116}	...	...	0	1
SWIFT J0854.7+1502	Seyfert 2	0.0696	...	$1.73^{+1.1}_{-1.5}$	19.7^{+13}_{-16}	...	...	>0.5[d]	1
Mrk 0704	Seyfert 1	0.0292	0.82[c]	$2.21^{+1.1}_{-0.9}$	$4.3^{+2.1}_{-1.8}$	114.9 ± 27.1	160	14.6	1
MCG -01-24-012	Seyfert 2	0.01964	2.86[c]	$4.6^{+0.7}_{-0.9}$	$3.7^{+0.4}_{-0.6}$	2914.4 ± 1092.9	nr	6.8	1
NGC 2992........................	Seyfert 1.9	0.00771	2.03	$3.6^{+1.0}_{-1.1}$	$0.47^{+0.13}_{-0.10}$	0.8 ± 0.1	520	0.17	1
ESO 434− G 040.............	Seyfert 2	0.00848	0.6	$19.1^{+0.6}_{-0.6}$	$2.7^{+0.1}_{-0.1}$	912.9 ± 21.1	85.5	1.5	1
3C 227	Seyfert 1	0.0858	5462	$2.23^{+0.3}_{-1.6}$	$40.0^{+1.0}_{-3.2}$	19.3 ± 7.10	nr	3.6	1
NGC 3081........................	Seyfert 2	0.00798	0.1[c]	$6.8^{+0.9}_{-0.8}$	$0.96^{+0.1}_{-0.11}$	31.0 ± 1.7	241	60	1

[a] The O III luminosities have been derived in Rau et al. (2007).
[b] Iron line equivalent width. A value of "nr" means that the iron line is statistically not required by the fit.
[c] The radio flux at other wavelengths has been extrapolated to 6 cm assuming $f_\nu \propto \nu^{-0.5}$.
[d] Limit on the absorption obtained extrapolating the BAT spectrum to the *ROSAT* band.
REFERENCES.—(1) this work; (2) Gallo et al. 2006; (3) Lutz et al. 2004.

only objects at $|b| > 15°$ that are not spatially associated with the Large Magellanic Cloud. Here we describe the main properties of the sample.

3.1. *Completeness of the Sample*

In order to compute the AGN number-flux relation, it is necessary to have a complete and unbiased sample. Since different regions of the sky have different exposure times, we applied in Ajello et al. (2007) a significance limit rather than a flux limit to define our sample. Now we want to test our extragalactic sample for completeness (i.e., derive the significance limit that is guaranteed to include all objects above a given flux limit), and we use the V/V_{max} method (Schmidt 1968).[5] This method, which is applied to samples complete to a well-defined significance limit, can also be used to test the completeness level of a sample as a function of significance. For a significance limit below the true completeness level limit of the sample, the V/V_{max} returns a value less than $\langle V/V_{max}\rangle_{true}$, which would be the true test result for a complete sample. Above the completeness limit the $\langle V/V_{max}\rangle$ values should be distributed around $\langle V/V_{max}\rangle_{true}$ within the statistical uncertainties.

V/V_{max} is computed for each source as $[F/(\sigma_{test}\delta F)]^{-3/2}$, where F is the flux, δF is the 1 σ statistical uncertainty, σ_{test} is the significance level tested for completeness (and thus the term $\sigma_{test}\delta F$ is the limiting flux of the sky region where we detected the source), and the exponent $-3/2$ comes from assuming no evolution and a uniform distribution in the local universe. $\langle V/V_{max}\rangle$

is computed as an average of all sources detected with S/N $\geq$ σ_{test}. For a given mean value $m = \langle V/V_{max}\rangle$ and n sources, the error on $\langle V/V_{max}\rangle$ can be computed as (Avni & Bahcall 1980):

$$\sigma_m(n) = \sqrt{\frac{1/3 - m - m^2}{n}}. \qquad (2)$$

The results of the test are shown in Figure 3. We find a constant value for significances >4.5 σ. The deviation from the expected 0.5 value is insignificant, being less than 1 σ.[6]

We also remark that for completeness we refer to the threshold above which all sources above the corresponding flux limit are included in the sample. Furthermore, given the small redshift of the sample (see § 3.3), the hypothesis of no evolution is justified.

3.2. *Extragalactic Source Counts*

The cumulative source number density can be computed as

$$N(> S) = \sum_{i=1}^{N_S} \frac{1}{\Omega_i} \; (\text{deg}^{-2}), \qquad (3)$$

where N_S is the total number of detected sources in the field with fluxes greater than S and Ω_i is the sky coverage associated to the flux of the ith source (shown in Fig. 9 of Ajello et al. 2007). The cumulative distribution is reported in Figure 4. We performed a maximum likelihood fit to the cumulative counts, assuming a

---

[5] In this test V stands for the volume where the object has been detected and V_{max} is the accessible volume in which the object, due to the flux limit of the survey, could have been found. In case of no evolution $\langle V/V_{max}\rangle = 0.5$ is expected.

[6] It is not uncommon for coded mask detectors to produce a test value slightly above 0.5 (e.g., Beckmann et al. 2006). This is likely caused by systematic errors which tend to increase the $\langle V/V_{max}\rangle$ value.
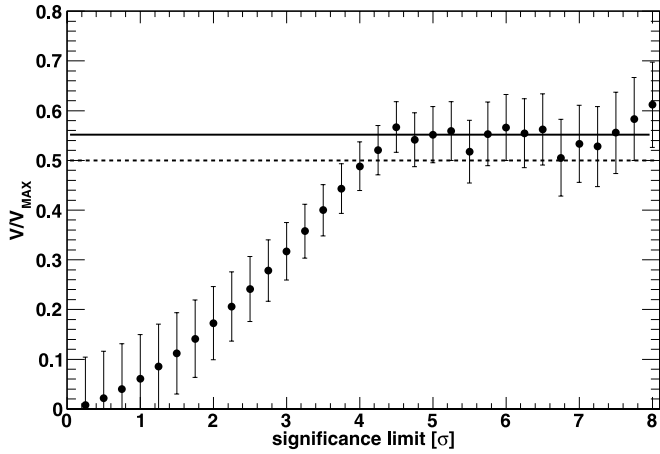
FIG. 3.—V/V_{max} as a function of detection threshold for the sample of extragalactic sources. The dashed line is the expected value (0.5) for a complete sample in an homogeneous distribution. The solid line shows the mean test value for S/N > 4.5 σ.

FIG. 4.—Extragalactic cumulative source count distribution in the 14–170 keV band. The solid line is the best fit described in the text.

simple power-law model of the form $N(> S) = AS^{-\alpha}$. Here A is the normalization at 2×10^{-11} ergs cm^{-2} s^{-1} and α is the slope. As is conventional, we used the maximum likelihood estimator (e.g., Crawford et al. 1970) to determine the best-fit values. The normalization is not a parameter of the fit but is obtained assuming that the number of expected sources from the best-fit model is equal to the total observed number. The Poissonian error on the total number of sources provides a reliable estimate of its error.

In the 14–170 keV band the best-fit parameter is $\alpha = 1.55 \pm 0.20$ (with normalization $9.6 \pm 1.9 \times 10^{-3}$ deg^{-2}). The source count distribution is thus consistent with a pure Euclidean function ($\alpha = 3/2$). From our data we expect that the number of all-sky AGNs brighter than 2×10^{-11} ergs cm^{-2} s^{-1} is 396 ± 80. This corresponds to an integrated flux of $\sim 5 \times 10^{-12}$ ergs cm^{-2} s^{-1} deg^{-2}, or $\sim 1.5\%$ of the intensity of the X-ray background in the 14–170 keV energy band as measured by *HEAO-1* (Gruber et al. 1999). We can compare the surface density of extragalactic objects found by BAT with previous measurements by converting the BAT fluxes to other energy bands, assuming a power-law spectrum with a photon index of 2.0 (see § 2) and evaluating the surface density above 10^{-11} ergs cm^{-2} s^{-1}.

The results of such comparisons are shown in Table 4. The BAT surface density is in agreement with the reported measurements, except for the case of the 0.5–2 and 2–10 keV surveys. Indeed, such surveys, at limiting fluxes of 10^{-11} ergs cm^{-2} s^{-1}, are biased against the detection of absorbed sources.[7] It is also worth noting that the recent *XMM-Newton* measurement of the 5–10 keV source counts distribution (Cappelluti et al. 2007) is in perfect agreement with our estimate.

3.3. *Statistical Properties*

Above the 4.5 σ the extragalactic sample, shown in Table 3, contains 24 AGNs. Nineteen objects are classified as Seyfert galaxies, 3 as blazars, 1 as an X-ray bright optically normal galaxy (XBONG), and 1 as a quasar. The identification completeness of such sample is thus 100%.

Excluding the blazars, the median redshift of the sample is $z = 0.026$ (the mean is $z = 0.046$), giving a median luminosity of $10^{43.5}$ ergs s^{-1} (the mean is $10^{43.8}$ ergs s^{-1}) in the 14–170 keV

---

[7] The bias decreases in deep fields and thus at lower fluxes (and higher redshifts) because the photoelectric cutoff is redshifted at lower energies.
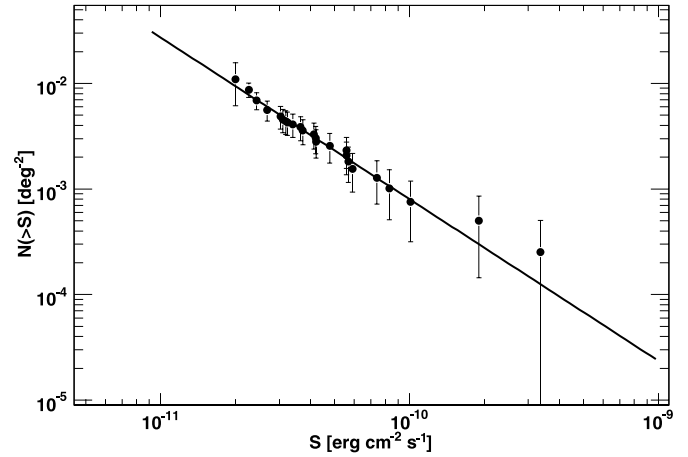
band. Assuming a hydrogen column density of 10^{22} atoms cm^{-2} as the threshold between absorbed and unabsorbed objects, we find that intrinsic absorption is present in $\sim 55\%$ of the sample. This fraction is lower than the 75% expected by the standard unified model, which is derived by the opening angle of ionizations cones (e.g., Evans et al. 1991). However, this unexpectedly low fraction of absorbed AGNs in the local universe does not seem to pose any particular problem for the understanding and the synthesis of the CXB (e.g., Sazonov et al. 2007).

In Figure 5 we show the intrinsic column density of the sources as a function of unabsorbed luminosity in the BAT band. Excluding the lower limits on the absorption, we do not find evidence of an anticorrelation between luminosity and absorption. We also note the presence of a rare very luminous ($L_x \sim 10^{45}$ ergs cm^{-2}) highly absorbed ($N_H \sim 10^{23}$ atoms cm^{-2}) type 2 QSO. If the lower limits on the absorption are confirmed, the total fraction of such objects might be in the range 5%–15%.

None of the sources in Table 3 with a 2–10 keV measurement is a Compton-thick AGN. Our claim is supported by several indications:

1. As shown by Matt et al. (1997) for NGC 1068, the spectra of Compton-thick AGNs might be reflection dominated (i.e., the reflection component is larger than the transmitted one). We thus tried to fit to each source a pure reflection model (`pexrav` in XSPEC). For all the sources, except Mrk 704, the fit is statistically unacceptable. However, Mrk 704 is not a Compton-thick source, as Landi et al. (2007) have recently shown.

2. Compton-thick sources generally show iron lines with equivalent widths of ~ 1 keV (e.g., Guainazzi et al. 2005). The spectral analysis (see also values in Table 3) shows that all sources have iron line equivalent widths smaller than 1 keV.

3. The thickness parameter T, defined as $L_{2-10\,keV}/L_{O\,III}$ (see also Bassani et al. 1999), can be used to identify Compton-thick sources (characterized by $T \leq 1$). We computed the thickness parameter for all sources with O III flux measurements (Rau et al. 2007) and 2–10 keV observations (see Table 3). All sources except NGC 2992 (which, however, is unabsorbed) have thickness parameter values consistent with the values expected for Compton-thin AGNs.

We evaluated the radio loudness of AGNs using the R-index defined in Laor (2000) as $R \equiv f_\nu(5\text{GHz})/f_\nu(4400\ \text{Å})$; the distribution of R-values has been shown to be bimodal, with a minimum at $R = 10$, commonly used to define radio-loud (above 10)

TABLE 4
COMPARISON WITH PREVIOUS RESULTS

Instrument	References	Energy (keV)	AGN Density[a] (10^{-2} deg^{-2})	BAT Density (this work)[b] (10^{-2} deg^{-2})
INTEGRAL ISGRI	1	20–40	0.48 ± 0.08	0.41 ± 0.08
INTEGRAL ISGRI	2	100–150	0.18 ± 0.006	0.17 ± 0.034
HEAO-1 A2	3	2–10	1.2 ± 0.2	1.6 ± 0.32
RXTE PCA	4	8–20	0.56 ± 0.06	0.65 ± 0.13
XMM-Newton	5	0.5–2	0.1 ± 0.01	1.3 ± 0.26
XMM-Newton	5	2–10	0.95 ± 0.06	1.6 ± 0.32
XMM-Newton	5	5–10	0.63 ± 0.4	0.4 ± 0.08

[a] AGN densities from different surveys above 10^{-11} ergs cm^{-2} s^{-1} (in the respective bands).
[b] The BAT AGN density was converted to the native energy band of the measurement we are comparing it with.
REFERENCES.—(1) Beckmann et al. 2006; (2) Bazzano et al. 2006; (3) Piccinotti et al. 1982; (4) Revnivtsev et al. 2004; (5) Cappelluti et al. 2007.

versus radio-quiet objects. Interestingly, we note that a relevant fraction (~40%) of the BAT AGNs is radio-loud and that these objects show a systematically harder X-ray spectra than Seyfert galaxies (mean of 1.66 vs. 2.00). There is large consensus that radio-loud quasars host more massive black holes than radio-quiet ones (e.g., Metcalf & Magliocchetti 2006; McLure & Jarvis 2004). However, there is no simple explanation for this radio-loudness dichotomy. Recently, Sikora et al. (2007) showed that the radio-loudness parameter inversely correlates with the Eddington ratio (fraction of bolometric to Eddington luminosity) for both spiral/disk and elliptical galaxies. The fact that spiral-hosted AGNs are radio-quiet at high accretion luminosities supports the idea that black hole spin plays a major role in the jet production (Sikora et al. 2007).[8] As confirmation, we find a good correlation of intrinsic X-ray luminosity and radio loudness (Spearman rank test of 0.57 with a probability of 0.003). Such a correlation is expected if there is a fundamental connection between accretion and jet activity (Merloni et al. 2003).

4. DISCUSSION

We have used the BAT X-ray survey to study key properties of the local ($z \leq 0.1$) AGN population. Our survey is based on the 14–170 keV fluxes and is sensitive to AGNs with column densities up to $N_H \sim 5 \times 10^{24}$ atoms cm^{-2}. Indeed, for a typical source

[8] In fact, by merging processes, black holes in elliptical galaxies are expected to have larger spins than those in spiral/disk galaxies.
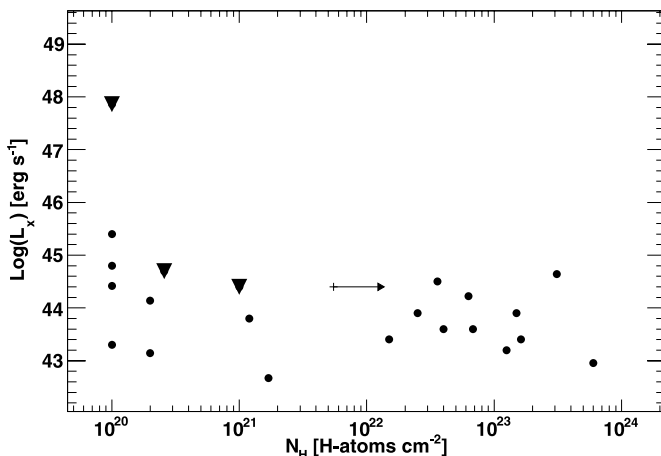
FIG. 5.—Luminosity, in the 14–170 keV band vs. intrinsic column density for the extragalactic sample. The blazars are highlighted with a triangle.

with a photon index of 2, the decrease in flux for column densities of $N_H \sim 10^{24}$ atoms cm^{-2} is only ~7% and ~55%[9] for column densities of $N_H \sim 3 \times 10^{24}$ atoms cm^{-2} . Thus, we can affirm that this survey is relatively unbiased with respect to photoelectric absorption.

Most of the population synthesis models (Ueda et al. 2003; Treister & Urry 2005; Gilli et al. 2007) predict that Compton-thick AGNs (log $N_H > 24$) provide a significant contribution to the bulk of the CXB emission at 30 keV (Marshall et al. 1980). Although studies of the local universe (e.g., Risaliti et al., 1999) have shown that Compton-thick objects should be as numerous as moderately obscured AGNs (log $N_H < 24$), and thus comprise roughly one-third of the total AGN population, only a handful of these sources are known (Comastri 2004). Gilli et al. (2007) estimate that the expected fraction of Compton-thick objects at limiting fluxes probed by BAT and *INTEGRAL* ($\sim 10^{-11}$ ergs cm^{-2} s^{-1}) is in the 15%–20% range. However, the measured fraction of detected Compton-thick objects by these instruments so far is close to or less than 10% (Markwardt et al. 2005; Beckmann et al. 2006).

The BAT extragalactic sample contains only one source, SWIFT J0823.4-0457, which, given its colors (see Fig. 1), might be Compton thick. However, the joint XRT and BAT spectra show that the absorption is below the Compton-thick level ($N_H \sim 10^{23}$ atoms cm^{-2}). We must therefore conclude that no Compton-thick AGNs are present in our extragalactic sample. The probability of not detecting Compton-thick objects in a sample of 24 AGNs when the expected fraction is 20% (15%) is ~0.007 (~0.03), while it is 0.1 if the expected fraction is 10%. These probabilities increase (0.03, 0.09, and 0.2 for the 20%, 15%, and 10% cases) if we assume that the only source that lacks a <10 keV measurement (J0854.7+1502) is Compton thick. Thus, the BAT data discard at the >2 σ level the hypothesis that Compton-thick AGNs may represent a fraction of ~20% of the total AGN population.

We find that Seyfert 2s have harder spectra than Seyfert 1s, in agreement with what has been deduced from *OSSE*, *BeppoSAX*, and *INTEGRAL* data (Zdziarski et al. 2000; Deluit & Courvoisier 2003; Beckmann et al. 2006, respectively). We tested whether this difference could be accounted for by Compton reflection and/or by a high-energy cutoff. We find that the reflection component improves the fit to the Seyfert 1 averaged spectrum (the *F*-test shows that the reflection is significant at more than the 92% level), but it leaves unaltered the photon index. Thus, the difference in

[9] Photoelectric absorption as well as Compton scattering has been taken into account in this estimate.

photon indices among Seyfert 1s and 2s cannot be ascribed solely to orientation effects (a stronger reflection is expected for face-on objects). The spectra of Seyfert 1s show hints of a spectral cutoff at ~100 keV, in agreement with Deluit & Courvoisier (2003). According to thermal Compton models, the absence of a cutoff in Seyfert 2s might indicate a higher temperature of the Comptonizing medium (with respect to Seyfert 1s) or that nonthermal Compton scattering plays an important role. Nevertheless, given the low signal-to-noise ratio (S/N) of our sources, our evidence for the cutoff in the Seyfert 1 spectra is weak.

The best power-law fit to the extragalactic source-counts distribution yields a slope of $\alpha = 1.55 \pm 0.20$, which is consistent with a Euclidean distribution. From the best fit, we derive a surface density of AGNs of $9.6 \pm 1.9 \times 10^{-3}$ deg^{-2} above the flux limit of 2×10^{-11} ergs cm^{-2} s^{-1}; this estimate is in very good agreement, when converted to the 20–40 keV band, with the recently derived source counts distribution based on *INTEGRAL* data (Beckmann et al. 2006). Beckmann et al. (2006) find a slope of 1.66 ± 0.11, which is also consistent with our measurement but steeper than the 1.5 Euclidean value. Even though this could be due to an imperfectly computed sky coverage, the authors suggest that the distribution of AGNs in the local universe may not be isotropic because of the local clustering of sources (e.g., the local group of galaxies).

The BAT source-count distribution resolves only 1%–2% of the CXB into extragalactic sources; nevertheless, as it is unbiased with respect to absorption, it gives important information relative to the fraction of obscured sources that are missed by deep <10 keV surveys because of absorption. The extrapolation of the BAT source-count distribution to the 2–10 keV band, assuming an unabsorbed spectrum with a photon index of 2, yields a surface density of AGNs of $1.6 \pm 0.32 \times 10^{-2}$ deg^{-2} above 10^{-11} ergs cm^{-2} s^{-1}; in contrast, the surface density as extrapolated to brighter fluxes by *XMM-Newton* (Cappelluti et al. 2007) and as predicted by the Gilli et al. (2007) model is 0.9×10^{-2} deg^{-2}. The factor of ~2 more sources seen by BAT can be explained in term of absorption. Indeed, if we take into account the absorption distribution derived for BAT AGNs by Markwardt et al. (2005) (thus assuming that 66% of all AGNs are absorbed with a mean column density of 10^{23} atoms cm^{-2}), we get a surface density of $0.86 \pm 0.17 \times 10^{-2}$ deg^{-2}, which is consistent with the *XMM-Newton* extrapolation and the model prediction.

The extragalactic sample is composed of ~90% emission-line galaxies and ~10% blazars. We find that 55% of the emission-line galaxies are obscured by absorbing columns larger than 10^{22} H atoms cm^{-2}. This fraction is in agreement with the *INTEGRAL* measurements (e.g., Sazonov et al. 2007) but is less than the value suggested (~75%) by the unified AGN model. However, Sazonov et al. (2007) successfully showed that low-luminosity (mostly absorbed) AGNs account for as much as ~90% of the luminosity density of the local universe. This finding is also confirmed by the Gilli et al. (2007) model, which shows that the required fraction of obscured sources varies with intrinsic luminosity, at 3.7 and 1.0 below and above $10^{43.5}$ ergs s^{-1}. A relevant fraction (~40%) of the BAT-detected AGNs are radio-loud. These objects show a systematically harder X-ray spectra than Seyfert galaxies (1.66 vs. 2.00). The hard photon index and the correlation of radio-loudness with X-ray luminosity suggest

that a jet is presently at work in all these objects. Our sample also comprises one (and possibly up to three, considering the *ROSAT* lower limits on the absorption) highly luminous highly absorbed QSOs.

5. SUMMARY

We use the *Swift* BAT instrument to study the properties of the local ($z \leq 1$) AGNs in connection with the synthesis of the X-ray background emission. The results of this study can be summarized as follows:

1. Despite the consensus that Compton-thick objects may represent a substantial fraction of the local AGN population (e.g., Risaliti et al. 1999; Gilli et al. 2007), we do not detect any such object. The probability associated to this nondetection is 0.007, 0.03, and 0.1, when assuming that their fraction should be 20%, 15%, and 10% of the total AGNs. BAT discards at >2 σ the hypothesis that the fraction of Compton-thick objects is 20%.

2. Seyfert 2 galaxies have harder X-ray spectra than Seyfert 1s. We find that this difference cannot be ascribed solely to the different viewing angle and thus to the different amount of Compton reflection expected. The Seyfert 1 galaxies included in our sample show weak evidence for a spectral cutoff in the ~100 keV range. This might highlight an intrinsic difference among the two classes. Indeed, the absence of a cutoff in the spectra of Seyfert 2s might indicate a different (higher) temperature of the Comptonizing medium or that nonthermal Compton scattering play an important role.

3. The best power-law fit to the extragalactic source counts is consistent with a Euclidean function with a slope of 1.55 ± 0.20. At the current limiting fluxes (2×10^{-11} ergs cm^{-2} s^{-1}), BAT resolves only 1%–2% of the CXB emission in the 14–170 keV band.

The fraction of emission-line AGNs that is absorbed by $N_H > 10^{22}$ atoms cm^{-2} is ~55%. This is lower than the 75% expected by the standard AGN unified model.

This work shows the capabilities of BAT to produce an unbiased sample of AGNs, which is important for the understanding of the synthesis of the CXB emission in the hard X-ray band.

APPENDIX

SPECTRAL EXTRACTION METHOD

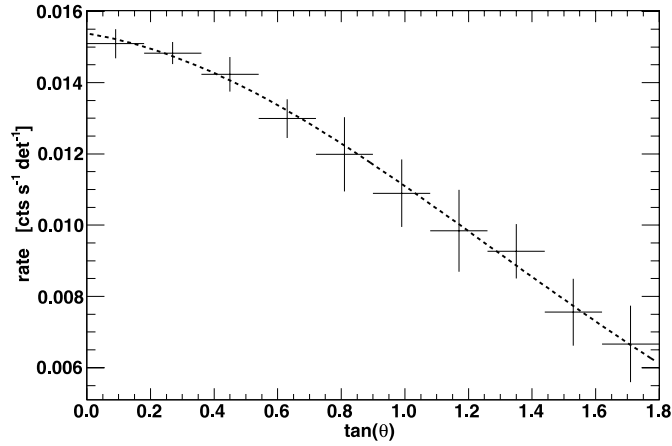We have developed a method to extract the averaged long-term spectrum of a source.

Fɪɢ. 6.—Crab Nebula rates in the 14–22 keV band as a function of the tangent of the off-axis angle. When the Crab is 50° off-axis the detected count rate is ∼30% lower than the on-axis count rate. The solid line is a polynomial fit to the rates.

In this method the spectrum is obtained as a weighted average of the source spectra of all observations in which the source is in the field of view (FOV). In particular, the averaged source count rates in the ith energy channel, $\bar{R}_i$, and their error $\bar{\sigma}_i$, are given by the following equations:

$$\bar{R}_i = \frac{\sum_{j=0}^{N} r_j * w_j}{\sum_{j=0}^{N} w_j},$$

$$\bar{\sigma}_i = \sqrt{\frac{\sum_{j=0}^{N} w_j V_j}{N \sum_{j=0}^{N} w_j}}, \tag{A1}$$

where r_j is the source count rate in the jth observation, w_j is the weight used, and the sums extend over all observations that contain the source. Using the inverse of the count rate variance V_j as a weight, the previous equations simplify to

$$\bar{R}_i = \frac{\sum_{j=0}^{N} r_j V_j^{-1}}{\sum_{j=0}^{N} 1/V_j},$$

$$\bar{\sigma}_i = \sqrt{\frac{1}{\sum_{j=0}^{N} 1/V_j}}. \tag{A2}$$

However, the spectra entering in equation (A2) must be corrected for off-axis count rate variation and for residual background contamination. We explain below the way these corrections are implemented.

A1. RATE VARIATION AS A FUNCTION OF OFF-AXIS ANGLE

The detected count rates strongly vary with the position of the source in the FOV; a source at the far edge of the partially coded FOV (PCFOV) can experience a decrease in rate of a factor of 2 (depending also on energy) compared to its on-axis rate.

The standard *Swift* BAT imaging software corrects for geometrical off-axis effects like cosine and partial coding (vignetting) effects; it is only when the response matrix is generated (with the tool `batdrmgen`) that other effects such as detector thickness and effective area variation are taken into account. Since in equation (A2) we are averaging over spectra at different positions in the FOV, we need to take into account the variations in the rates produced by the detector response. In order to do so, we have analyzed a series of more than 1000 Crab Nebula observations. For each of our six energy channels we made a polynomial fit to the Crab rate as a function of the off-axis angle and derived a set of corrective coefficients. These coefficients are then used to correct the rates of each source spectrum in order to transform them to the equivalent on-axis rates. The variation of the Crab rates as a function of position in the FOV is reported in Figure 6.

A2. RESIDUAL BACKGROUND CONTAMINATION

In order to extract a source spectrum from survey data (in form of detector plane histograms [DPHs]) the user must first produce a mask of weights (tool `batmaskwtimg`) for the source position and then use this mask to extract the detected counts from the array (tool `batbinevt`). The weights are chosen such that the resulting spectrum is already background subtracted. This is an implementation of the standard mask-weighting technique called *balanced correlation* (Fenimore & Cannon 1978). The automatic background subtraction works as long as the noise in the array is flat and not correlated with the mask pattern. These conditions are not always satisfied and a small background contamination can arise.

The total background contamination for the case of the Crab Nebula is <2% when compared to the Crab on-axis rate in the 14–195 keV band. Thus, this contamination does not pose problems for bright sources. However, it becomes relevant for the spectral analysis of faint
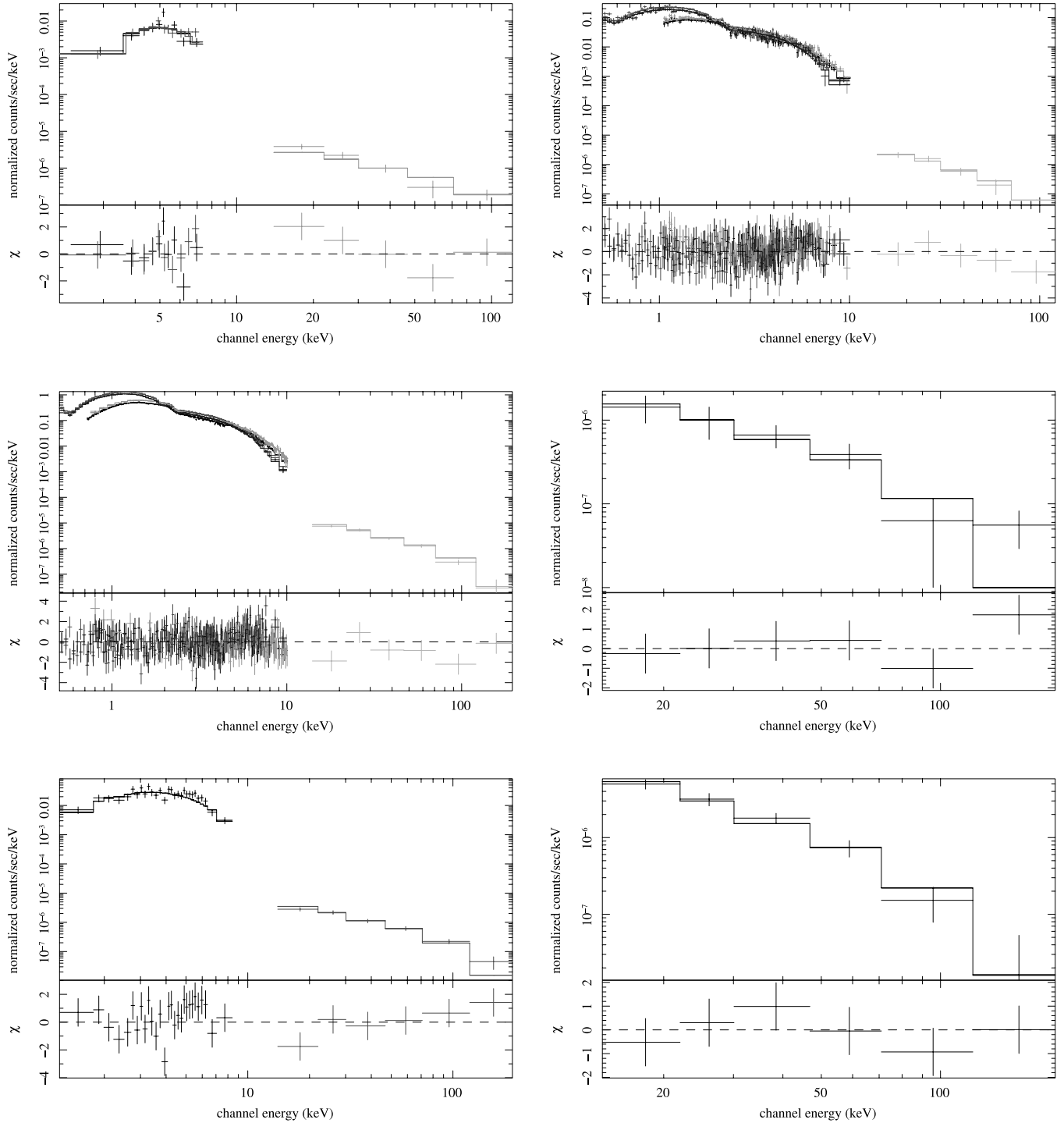
Fig. 7.—Folded spectra and best-fit models as described in the text. From left to right and top to bottom the spectra are for 3C 105.0, 1AXG J042556−5711, 3C 120, MCG-01-13-025, SWIFT J0505.7−2348, and CSV 6150. [*See the electronic edition of the Journal for a color version of this figure.*]

objects with intensities of ∼millicrab. To correct for this residual background contamination, we fit the `batclean` background model to each energy channel in order to create a background prediction for each of them. Convolving these background predictions with the mask of weights generated for the source under analysis yields the residual background term which the mask-weighting technique did not manage to suppress.

A3. SPECTRAL FITTING

The final source rates in the ith energy channel are computed as

$$\bar{R}_i = \frac{\sum_{j=0}^{N}(r_j - b_j)K(E,\ \theta)1/V_j}{\sum_{j=0}^{N}1/V_j},$$

$$(A3)$$
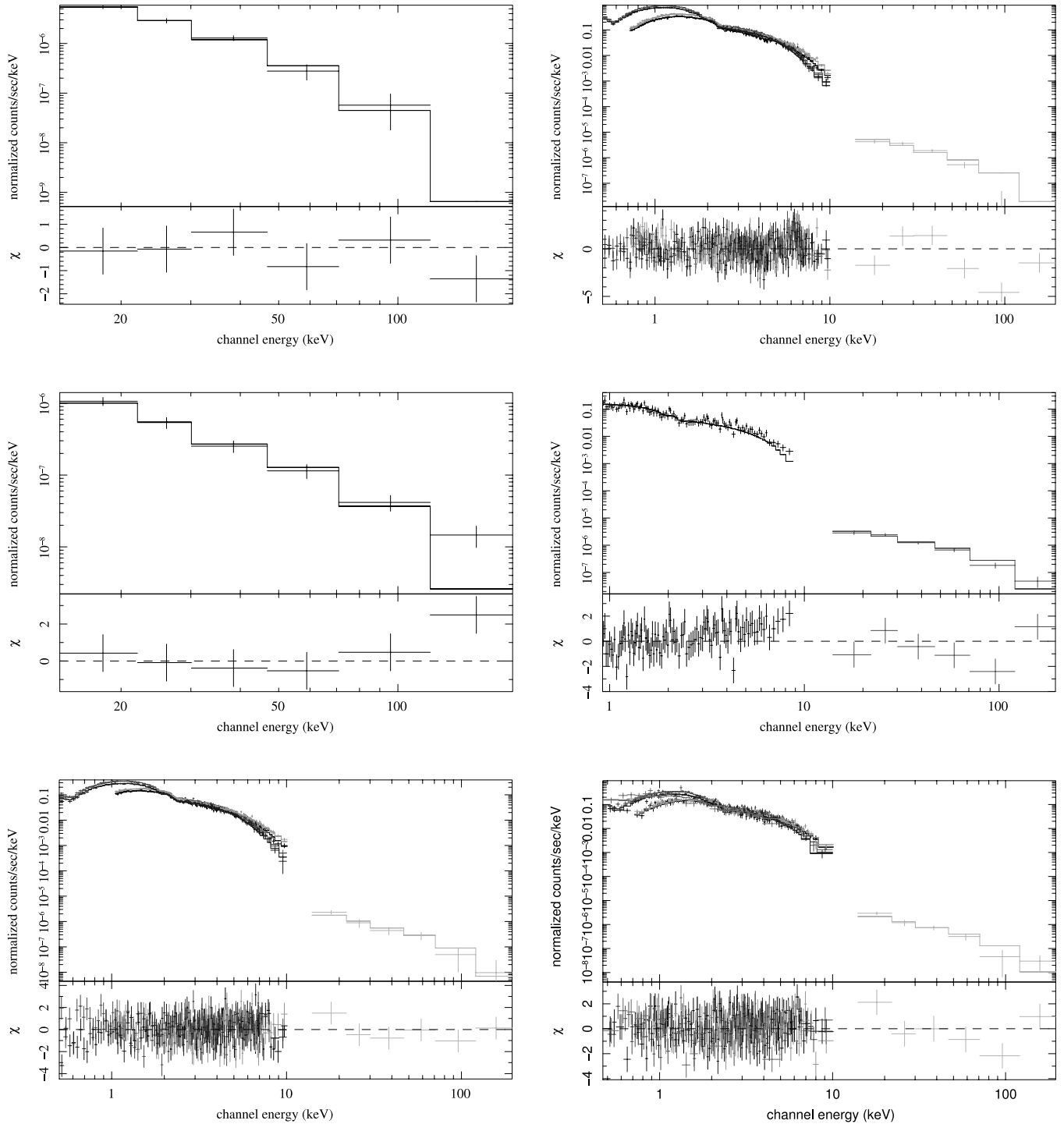
Fig. 8.—Same as Fig. 7, but for 4U 0513-40, QSO B0513-002, SWIFT J0517.1+1633, ESO 362-G 018, Pictor A, and ESO 362-G 021. [*See the electronic edition of the Journal for a color version of this figure.*]

where b_j is the residual background term, $K(E, \theta)$ is the parametrized instrumental response as function of the energy channel and the off-axis angle, and V_j is the rate variance. The weighted averaged spectrum is then input, together with a BAT response matrix, to XSPEC 11.3.2 (Arnaud 1996) for spectral fitting.

Finally, we check that the averaged Crab Nebula spectrum obtained with the above method is consistent with the standard (BAT) Crab spectrum as detected in each observation (photon index of 2.15 and normalization of 10.15 photons cm^{-2} s^{-1} at 1 keV in the 15–200 keV energy range).

A4. NOTES ON INDIVIDUAL SOURCES

We report a brief description of the source spectra for all new or interesting sources found in this analysis. All quoted errors are 90%. The spectra of all the sources are reported in Figures 7, 8, 9, 10, 11, 12, 13, and 14.
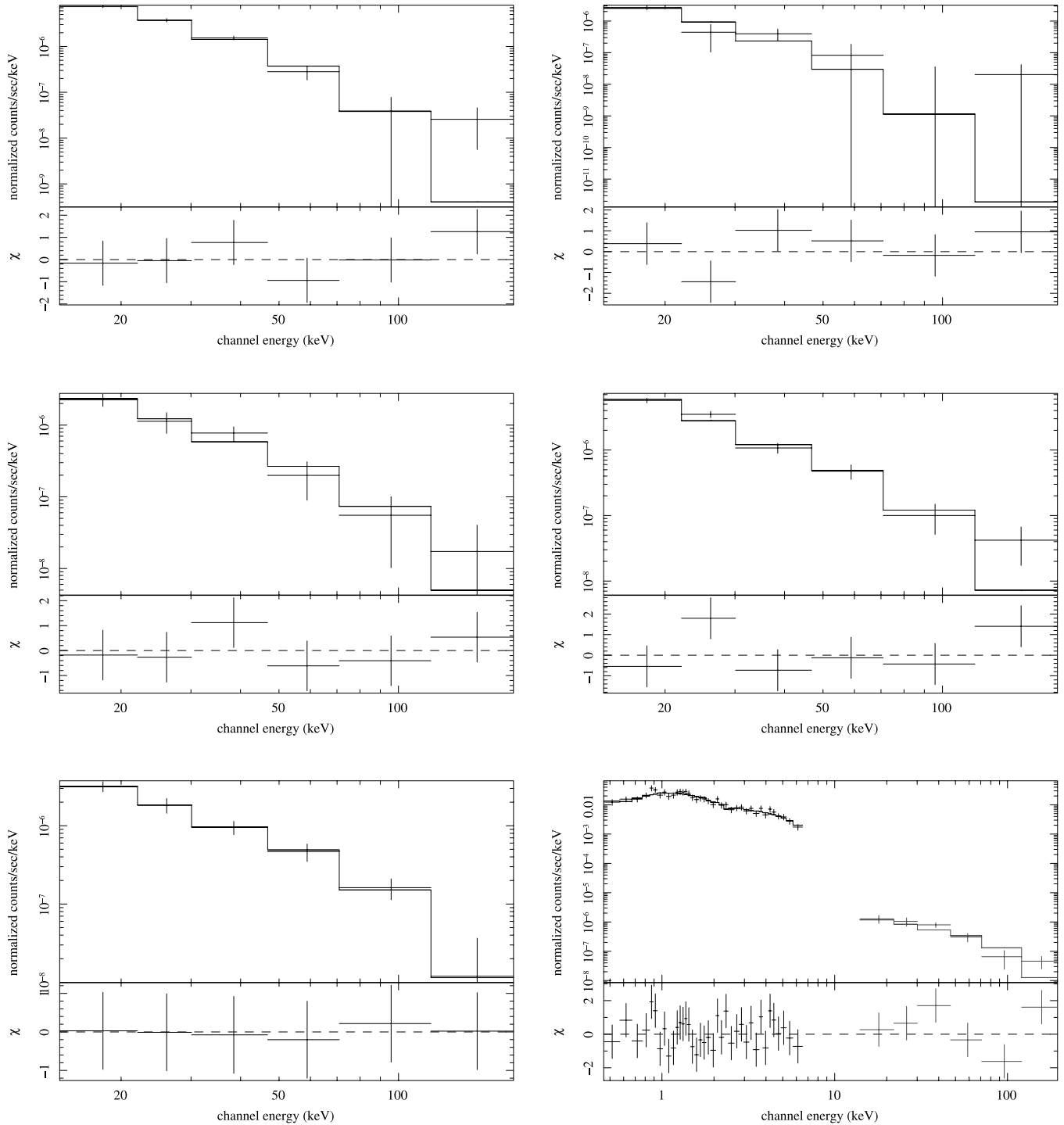
Fig. 9.—Same as Fig. 7, but for TV Col, TW Pic, LMC X-3, LMC X-1, PSR B0540-69.3, and PKS 0537-286. [*See the electronic edition of the Journal for a color version of this figure.*]

3C 105.0 is a Seyfert 2 galaxy. The BAT and XRT data can be fit by an absorbed power-law model with a photon index of 1.65 ± 0.13 and a hydrogen column density of $29.4^{+5.7}_{-4.8} \times 10^{22}$ atoms cm^{-2}. Given its absorption and its luminosity (4.45×10^{44} ergs s^{-1}), 3C 105.0 is a highly absorbed highly luminous QSO.

1 AXG J042556-5711 (also known as 1H 0419-577, LB 1727, 1ES 0425-573, and IRAS F04250-5718) is a radio-quiet Seyfert galaxy which has been observed over recent years by *ASCA*, *ROSAT*, *BeppoSAX*, and recently also by *RXTE* (Revnivtsev et al. 2006). The *ASCA* and BAT data are well fit by an unabsorbed cutoff power-law model with a photon index of 1.54 ± 0.028 and cutoff at $73^{+46.2}_{-24.1}$ keV.

3C 120 is a Seyfert 1 galaxy. This source was observed by *ASCA*. The best fit to *ASCA* and BAT data is an absorbed power-law model with absorption consistent with the Galactic one, a photon index of $1.80^{+0.04}_{-0.04}$, and a blackbody component with a temperature of $0.27^{+0.026}_{-0.025}$ keV.

MCG-01-13-025 is a Seyfert 1.2 (in NED, but Seyfert 1 in SIMBAD) galaxy detected in soft X-rays by *ROSAT* (Voges et al. 1999). The BAT spectrum is consistent with a power law with a photon index of $1.6^{+0.48}_{-0.47}$ and it extends up to 200 keV.
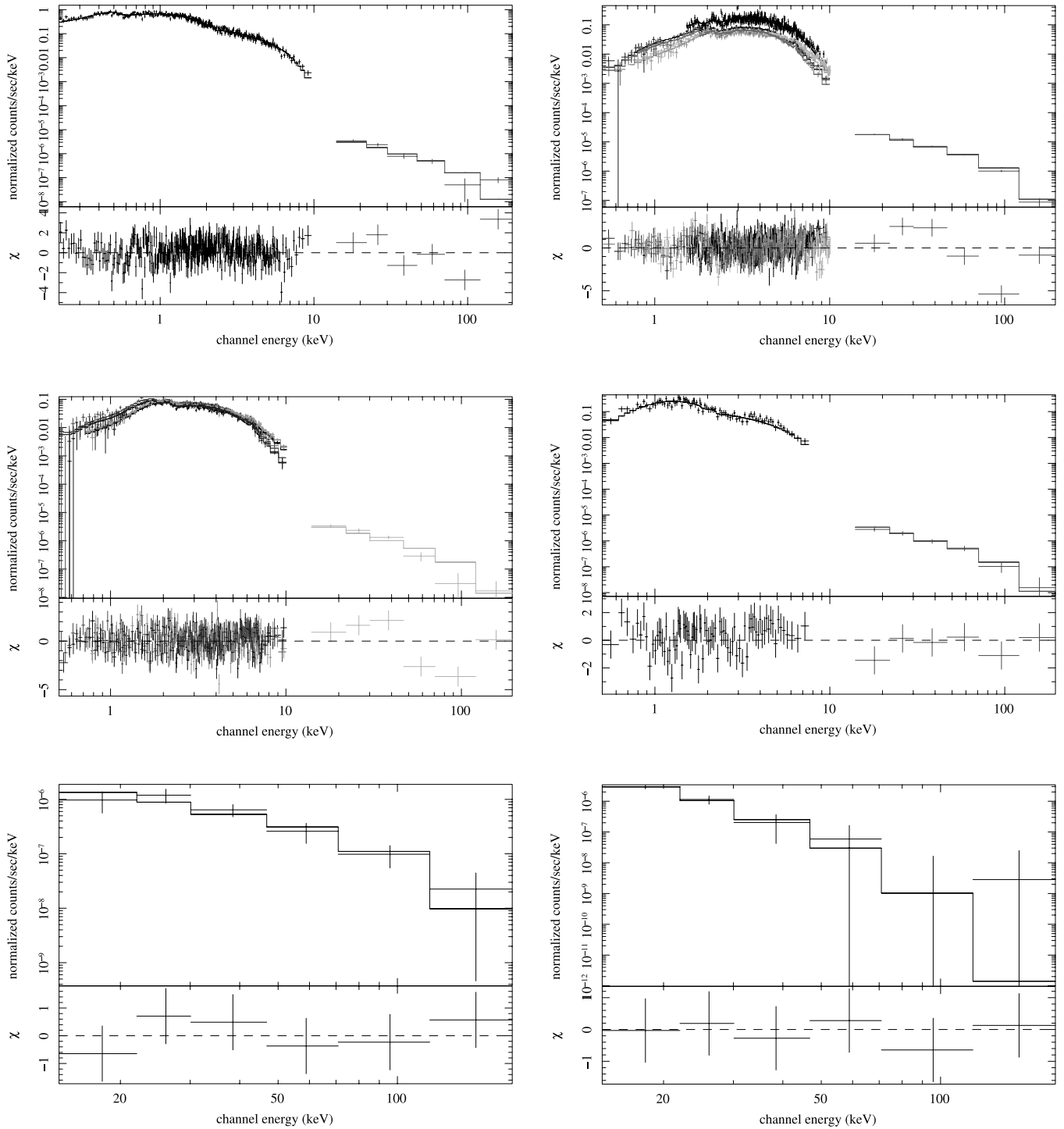
Fig. 10.—Same as Fig. 7, but for PKS 0548−322, NGC 2110, LEDA 75476, ESO 490-G26, J0727.5−2406, and V441 Pup. [*See the electronic edition of the Journal for a color version of this figure.*]

SWIFT J0505.7−2348, also know as XSS J05054−2348 (Revnivtsev et al. 2006), is a Seyfert 2 galaxy. When combining both XRT and BAT data for this source we get an intrinsic, rest-frame absorption of $4.8^{+0.9}_{-0.7} \times 10^{22}$ atoms cm^{-2} and a photon index of $1.77^{+0.08}_{-0.07}$.

CSV 6150, also known as IRAS 05078+1626, is cataloged as Seyfert 1 in SIMBAD and as Seyfert 1.5 in NED. The BAT spectrum can be fit with a power law with a photon index of $1.94^{+0.25}_{-0.23}$. The source flux in the 14–170 keV band is $6.3^{+0.7}_{-4.0} \times 10^{-11}$ ergs cm^{-2} s^{-1}, while the luminosity is $4.4^{+0.6}_{-2.2} \times 10^{43}$ ergs s^{-1}.

4U 0513-40 is a low-mass X-ray binary detected in X-rays by *EXOSAT* (Giommi et al. 1991). The BAT spectrum can be fit by a bremsstrahlung model with temperature of $29.7^{+7.5}_{-5.8}$ keV.

QSO B0513−002 is a Seyfert 1 galaxy. The BAT and *ASCA* spectra can be fit by an absorbed power-law model and a blackbody component. The required absorption is in agreement with the Galactic one. The photon index and the plasma temperature are, respectively, $1.83^{+0.02}_{-0.016}$ and $0.27^{+0.02}_{-0.02}$ keV. We also detect an iron line whose equivalent width is $90.8^{+66.2}_{-76.7}$ eV.
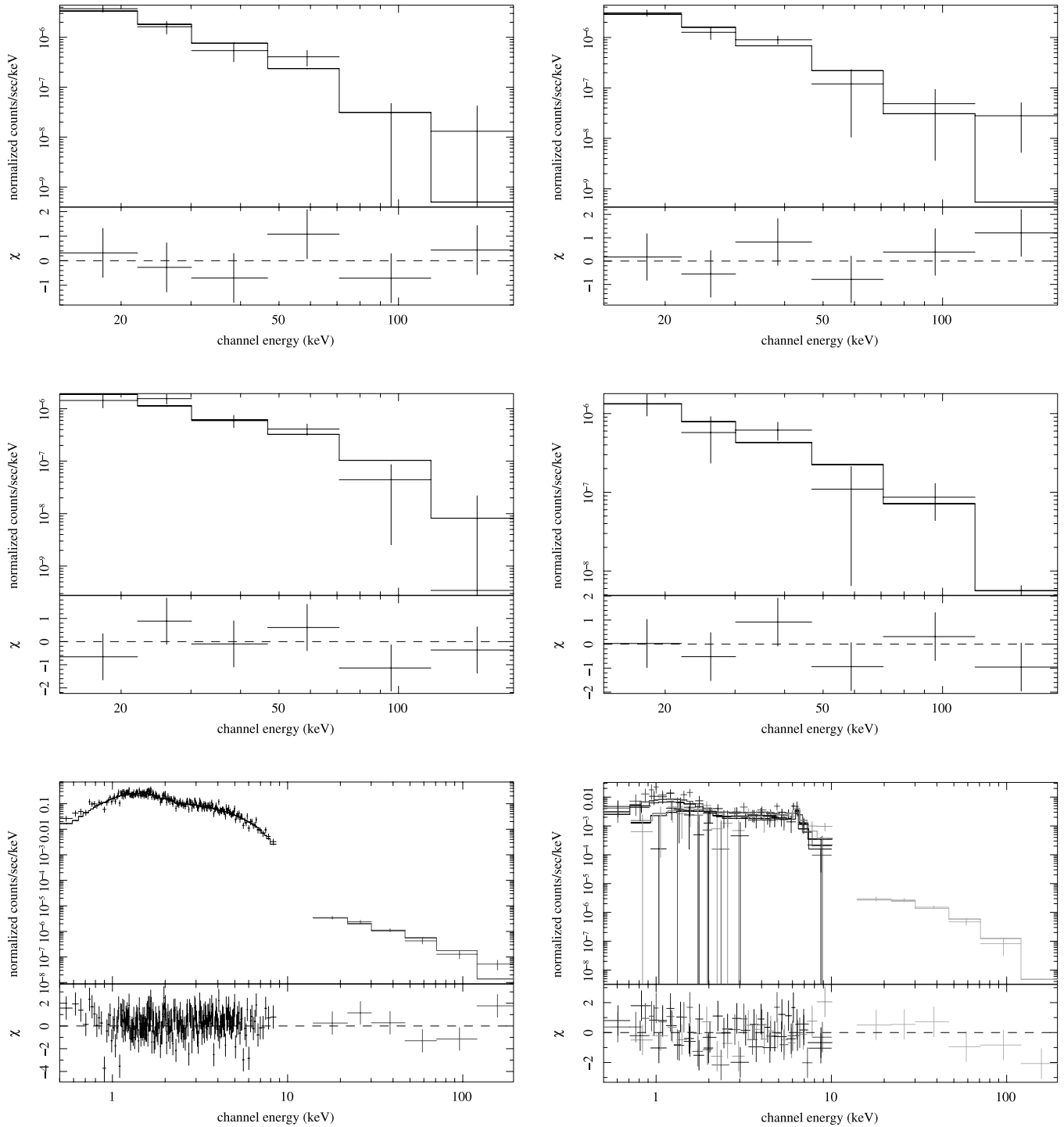
FIG. 11.—Same as Fig. 7, but for BG CMi, J0732.5−1331, J0739.6−3144, J0743.0−2543, IGR K07597−3842, and UGC 4203. [*See the electronic edition of the Journal for a color version of this figure.*]

SWIFT J0517.1+1633 is a new hard X-ray source (Ajello et al. 2007). The BAT spectrum is best fit by a power-law model with a photon index of $2.0^{+0.23}_{-0.26}$.

ESO 362-G018 is a Seyfert 1 galaxy detected at hard X-ray by BAT (Tueller et al. 2005). The BAT and XRT data are best fit by an absorbed power-law model with a photon index of $1.50^{+0.03}_{-0.02}$ and absorption consistent with the Galactic value.

Pictor A is a radio-loud Seyfert 1 galaxy initially detected in X-ray by the *Einstein* observatory (Elvis et al. 1992). The best fit to *ASCA* and BAT data is an absorbed power-law model with a photon index of $1.8^{+0.02}_{-0.02}$ and intrinsic absorption of $1.14^{+0.01}_{-0.05} \times 10^{21}$ atoms cm^{-2} slightly in excess of the Galactic one (4×10^{20} atoms cm^{-2}).

ESO 362-G021 is a BL Lac object. *ASCA* and XRT data are available for this source. The best fit to *ASCA*, BAT, and XRT data is an absorbed power law with a photon index of $1.72^{+0.04}_{-0.04}$ and an intrinsic column density of $0.14^{+0.02}_{-0.02} \times 10^{22}$ atoms cm^{-2}.

TV Col is a DQ Her–type cataclysmic variable already detected at soft and hard X-rays. A power-law fit to the BAT spectrum does not yield acceptable results; instead a bremsstrahlung model with a plasma temperature of $28.2^{+4.6}_{-3.8}$ keV fits the data well.
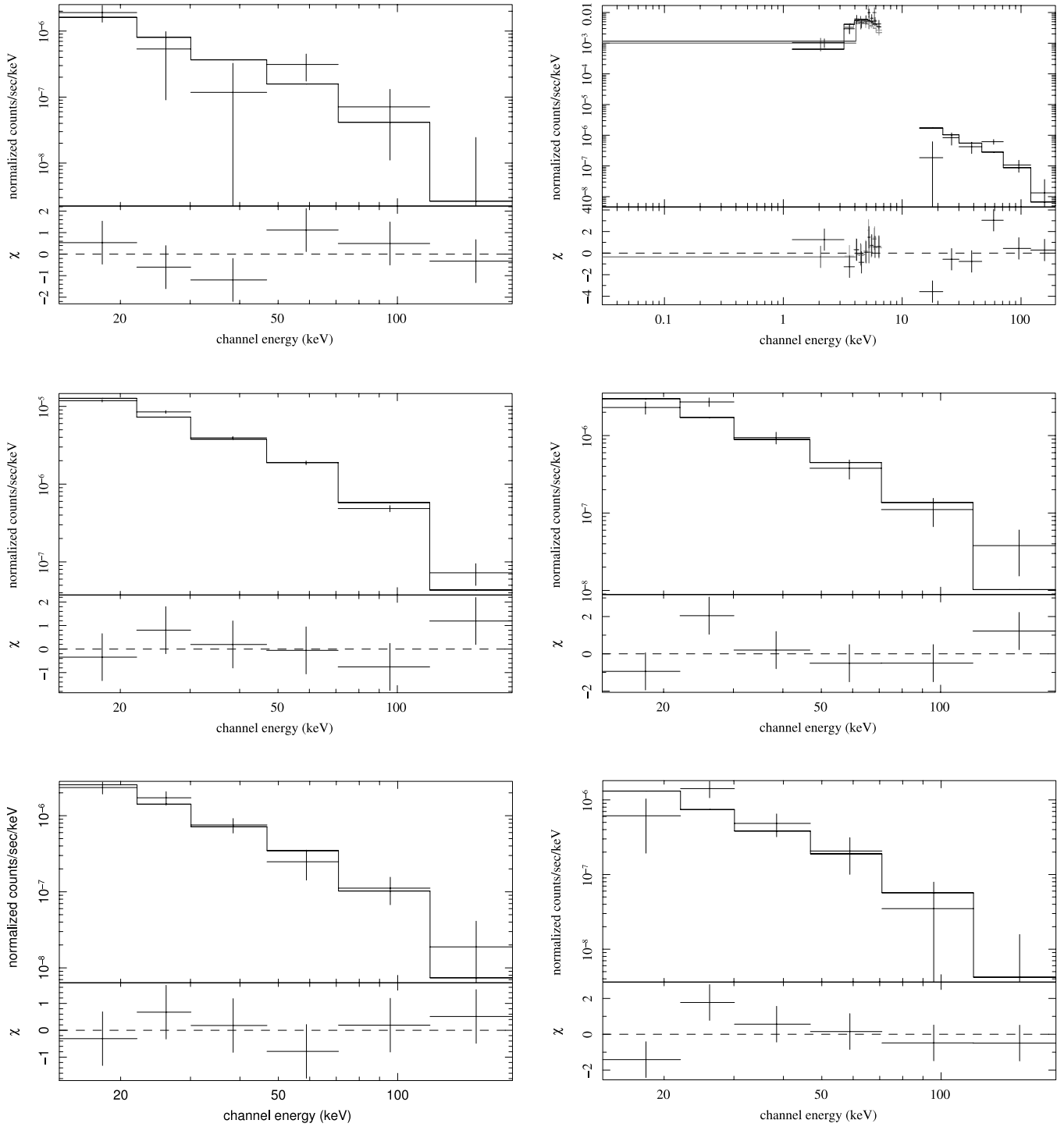
Fig. 12.—Same as Fig. 7, but for J0811.5+0937, J0823.4−0457, VELA PSR, FRL 1146, 3C 206, and J0844.9−3531. [*See the electronic edition of the Journal for a color version of this figure.*]

TW PIC is a cataclysmic variable of the DQ Her type (Norton et al. 2000). The BAT spectrum is best fit by a bremsstrahlung model with a plasma temperature of $13.5^{+10.6}_{-5.6}$ keV. The flux of 5.5×10^{-12} ergs cm^{-2} s^{-1} in the 20–40 keV band is a factor 2 lower than the one reported in a recent *INTEGRAL* measurement (Götz et al. 2006), suggesting variability.

LMC X-3 is a high-mass X-ray binary (HXB). The BAT spectrum is consistent with a power law whose photon index is $2.0^{+0.4}_{-0.3}$.

LMC X-1 is a well-known black hole candidate. It is detected up to 200 keV with a steep photon index of $2.3^{+0.22}_{-0.20}$. The flux is a factor 2 lower than the one measured by *INTEGRAL* (Götz et al. 2006), suggesting variability.

PSR B0540−69.3 is a young rotation-powered pulsar recently detected up to 60 keV also by *INTEGRAL* (Götz et al. 2006; Slowikowska et al. 2006). The pulsar is detected in BAT up to 200 keV and its spectrum can be modeled as a power law with a photon index of $1.85^{+0.28}_{-0.26}$.

PKS 0537−286 at $z = 3.1$ is one of the most luminous high-redshift quasars. Recognized first as a radio source (Bolton & Butler 1975), it was discovered in X-rays by the *Einstein* observatory (Zamorani et al. 1981) and then studied by *ROSAT*, *ASCA*, and lately by
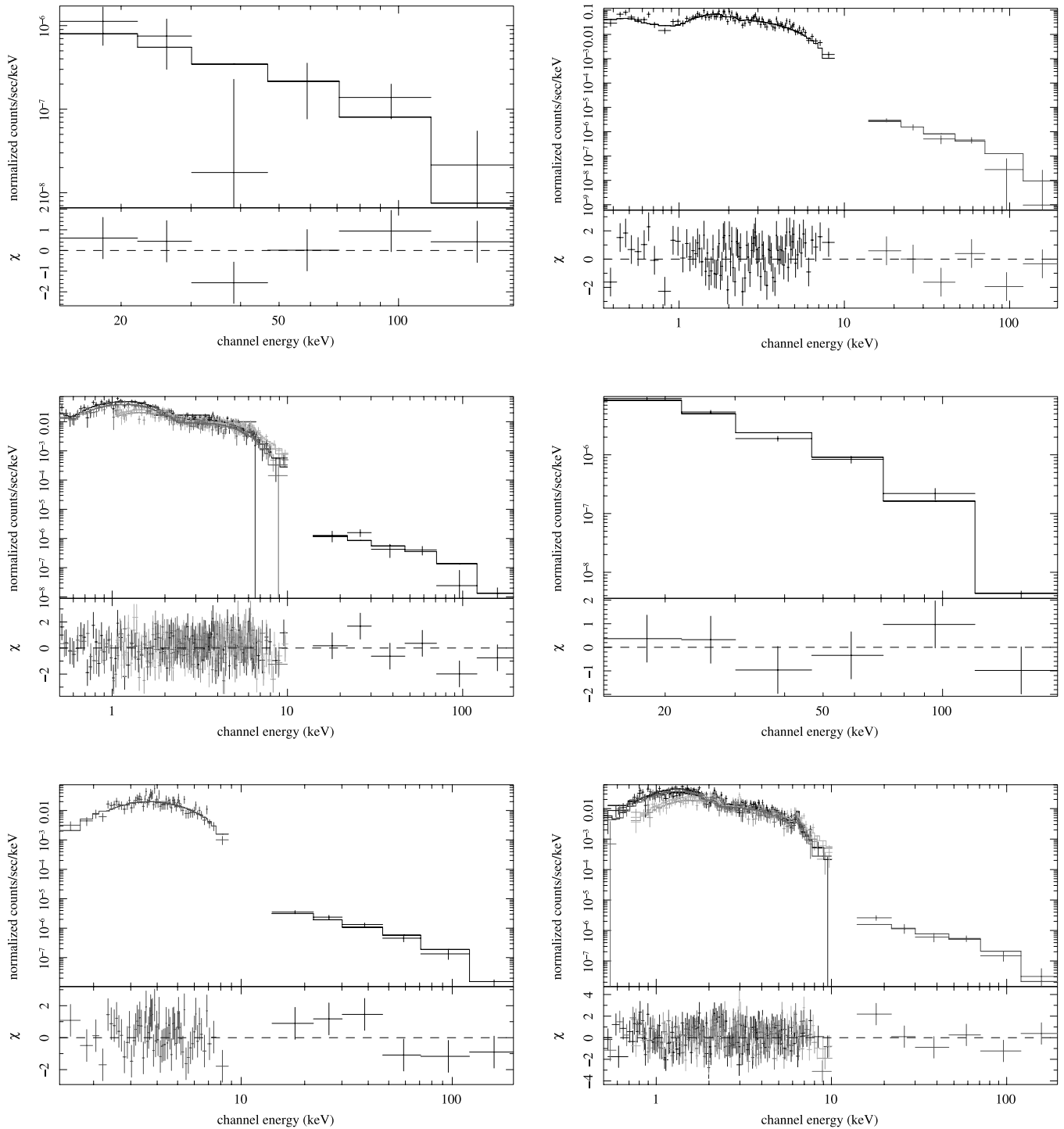
FIG. 13.—Same as Fig. 7, but for J0854.7+1502, J0917.2−6221, Mrk 704, 4U 0919-54, MCG -01-24-012, and NGC 2992. [*See the electronic edition of the Journal for a color version of this figure.*]

XMM-Newton. The BAT detection in hard X-rays is the first to date; however, a claim has been made that PKS 0537−286 is the MeV counterpart of the EGRET source 3EG J0531−2940 (Sowards-Emmerd et al. 2004). A joint spectral fit to XRT and BAT data reveals an exceptionally hard spectral slope of $1.35^{+0.06}_{-0.08}$.

PKS 0548−322 is a well-known blazar already detected in hard X-rays (see, for example, Donato et al. 2005). A joint spectrum of XRT and BAT data with an absorbed power-law model yields a photon index of $1.8^{+0.03}_{-0.03}$ and an intrinsic absorption of $2.57^{+0.6}_{-0.5} \times 10^{20}$ atoms cm^{-2}.

NGC 2110 is a well-known Seyfert 2 galaxy. The BAT, *ASCA*, and XRT data can be fit by an absorbed power-law model (photon index of $1.62^{+0.01}_{-0.01}$ and an intrinsic hydrogen column density of $4.0^{+0.13}_{-0.07} \times 10^{22}$ atoms cm^{-2}) with a soft excess which could be described as blackbody component with temperature of $0.47^{+0.02}_{-0.02}$. We also detected an unresolved Fe Kα of equivalent width of 118^{+42}_{-53} eV.

LEDA 75476, also known as 3A 0557-383, EXO 055620-3820.2, and CTS B31.01, is a Seyfert 1 galaxy. The BAT spectrum is consistent with a power-law model with a photon index of 2.0 ± 0.4. The *ASCA* and BAT data are well fit by an absorbed power-law
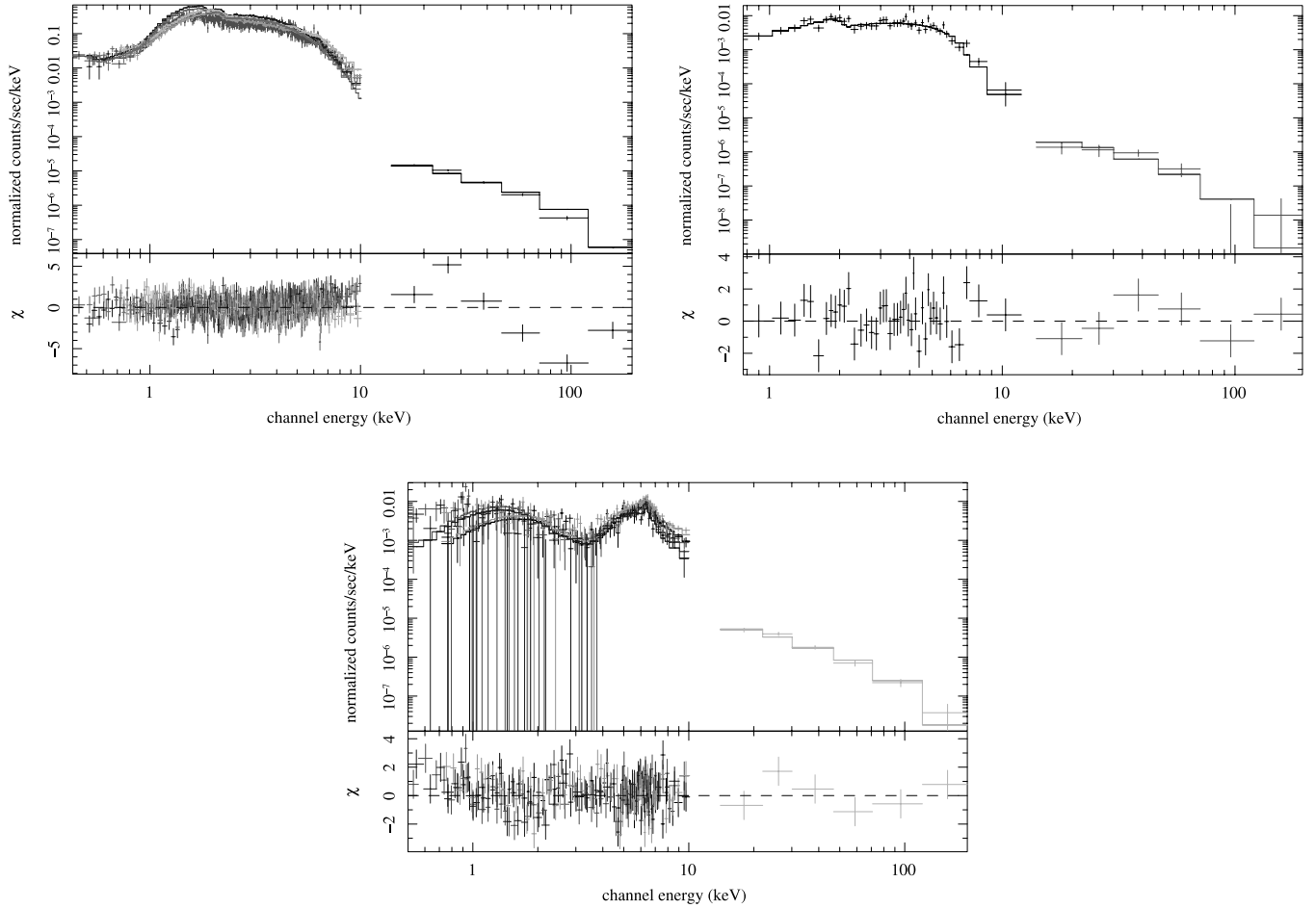
Fig. 14.—Folded spectra and best-fit models as described in the text. From left to right and up to bottom the spectra are for: ESO 434−G040, 3C 227, and NGC 3081. [*See the electronic edition of the Journal for a color version of this figure.*]

model with a photon index of $1.74^{+0.02}_{-0.03}$ and an intrinsic absorbing column density of $2.2^{+0.11}_{-0.13} \times 10^{22}$ atoms cm^{-2}. A clear excess below 2 keV is detected in the *ASCA* data, and this can be modeled as a blackbody component with a temperature of $0.28^{+0.08}_{-0.05}$ keV. A Fe Kα line is also required by the fit (with an *F*-test yielding a probability of the line being spurious of 10^{-8}), and its equivalent width is 0.132 keV. The reduced χ^2 of the overall fit is 1.1.

ESO 490-G26 is a Seyfert 1.2 galaxy. The joint XRT-BAT spectrum can be described as a power law with a photon index of $1.90^{+0.05}_{-0.04}$ and an intrinsic, in addition to Galactic, absorption of $2.7^{+0.05}_{-0.05} \times 10^{21}$ atoms cm^{-2}. The flux and the luminosity in the 14–170 keV band are $3.6^{+1.1}_{-1.3} \times 10^{-11}$ ergs cm^{-2} s^{-1} and $4.7^{+1.2}_{-3.6} \times 10^{43}$ ergs s^{-1}.

SWIFT J0727.5−2406 has a spectrum consistent with a power-law model with a photon index of 1.53 ± 0.54. As already noted by Rau et al. (2007), this BXS source is likely associated with the nearby *ROSAT* source 1RXS J072720.8−240629 and with the radio object NVSS J072721−240632.

V441 Pup is a high-mass X-ray binary for which the companion was optically identified as a Be star. The BAT spectrum is very steep and it can either be fit by a power law with a photon index of 4.5 ± 1.5 or by a bremsstrahlung model with a plasma temperature of $12.4^{+13.6}_{-5.6}$ keV.

BG CMi is a well-known intermediate polar. The BAT spectrum is consistent with a bremsstrahlung model with a plasma temperature of $31.3^{+41.2}_{-14.2}$ keV.

SWIFT J0732.5−1331 was detected for the first time by BAT in hard X-rays (Ajello et al. 2006). It was then identified as a new intermediate polar (Wheatley et al. 2006 and references therein). The BAT spectrum is consistent with a bremsstrahlung model with a plasma temperature of $33.2^{+50.1}_{-14.2}$ keV.

SWIFT J0739.6−3144 is a newly discovered hard X-ray source (Ajello et al. 2007), recently identified as a Seyfert 2 galaxy (Rau et al. 2007). A simple power-law fit to the BAT spectrum yields a photon index of $1.77^{+0.51}_{-0.43}$. We also estimated the lower limit on the absorbing column density considering the nondetection by *ROSAT*; this limit is $\sim 2 \times 10^{22}$ atoms cm^{-2}. The flux and the luminosity in the 14–170 keV band are $2.3^{+1.1}_{-1.8} \times 10^{-11}$ ergs cm^{-2} s^{-1} and $3.2^{+1.6}_{-1.9} \times 10^{43}$ ergs s^{-1}.

SWIFT J0743.0−2543 is a newly discovered hard X-ray source (Ajello et al. 2007). The BAT spectrum is consistent with a power-law model with a photon index of $1.78^{+0.69}_{-0.56}$. As noted in Rau et al. (2007) this BXS source is likely to be associated with the *ROSAT* source 1RXS J074315.6−254545 and the galaxy LEDA 86073.

IGR J07597−3842 is a source first detected by *INTEGRAL* in the VELA region (den Hartog et al. 2004). It was identified as being a Seyfert 1.2 (Masetti et al. 2006b). This source was also observed by XRT and when jointly fitting XRT and BAT data we find that the best fit is an absorbed power law with a photon index of $1.8^{+0.08}_{-0.07}$ and a column density of $5.8^{+0.5}_{-0.5} \times 10^{21}$ atoms cm^{-2}, consistent with the

Galactic foreground absorption. The source is thus unabsorbed. The flux and the luminosity in the 14–170 keV band are $4.2^{+0.6}_{-2.4} \times 10^{-11}$ ergs cm^{-2} s^{-1} and $15.9^{+1.5}_{-14.8} \times 10^{43}$ ergs s^{-1}.

UGC 4203 is a Seyfert 2 galaxy. As already noted in Matt et al. (2003), this source shows transitions between a reflection-dominated and a transmission-dominated spectrum. The *ASCA* and BAT data can be successfully fit by a reflection model (pexrav; Magdziarz & Zdziarski 1995) with a photon index of 1.68 ± 0.1 and a reflection normalization of $65.2^{+43.2}_{-23.07}$ and a prominent iron line with equivalent width of $0.7^{+1.1}_{-0.6}$ keV. A soft excess at energies <1 keV can be modeled as a blackbody component with a temperature of $0.3^{+0.08}_{-0.05}$ keV. XRT data are also available for this source. However, the XRT spectrum has a lower quality than the *ASCA* one. In the XRT observation, the source is found in a transmission-dominated state; the best-fit model is an absorbed reflection model (the reflection component is required by the BAT spectrum) with a hydrogen column density of $N_{\rm H} = 12.5^{+5.0}_{-3.7} \times 10^{22}$ atoms cm^{-2}, a photon index of $2.0^{+0.25}_{-0.25}$, and a reflection normalization of $2.12^{+2.5}_{-1.5}$.

SWIFT J0811.5+0937 is a new BXS source detected by Ajello et al. (2007). The BAT spectrum is consistent with a power law with a photon index of $2.2^{+2.1}_{-0.9}$. Rau et al. (2007) identified RX J081132.4+093403 as a possible counterpart. Optical spectroscopy revealed that this source is a candidate X-ray bright optically normal galaxy (XBONG). If we extrapolate the BAT power law to the *ROSAT*-PSPC energy band (0.1–2.4 keV), we get no indication of intrinsic absorption.

SWIFT J0823.4−0457 is a source detected for the first time in hard X-rays by BAT and associated, during an XRT follow-up, with the galaxy FAIRALL 0272 (Ajello et al. 2007). An optical follow-up showed that the source is a Seyfert 2 (Masetti et al. 2006a). XRT and BAT data are best fit by a highly absorbed power law. The photon index is $1.84^{+0.28}_{-0.22}$ and the absorbing column density is $19.3^{+6.8}_{-5.4} \times 10^{22}$ atoms cm^{-2}.

Vela PSR has a spectrum consistent with a power law whose photon index is 1.88 ± 0.2.

FRL 1146 is a Seyfert 1 galaxy detected in hard X-rays by *INTEGRAL* (Bird et al. 2006). The BAT spectrum is characterized by a power law with a photon index of $1.88^{+0.37}_{-0.31}$ extending up to 200 keV. The 14–170 keV flux and luminosity of $3.3^{+0.8}_{-0.7} \times 10^{-11}$ ergs cm^{-2} s^{-1} and $7.2^{+1.6}_{-1.4} \times 10^{43}$ ergs s^{-1} are in agreement with the *INTEGRAL* measurement. FRL 1146 was also detected in the *ROSAT* all-sky survey at 12 count s^{-1}; considering the extrapolation of the BAT power law to the *ROSAT* band yields ~8 count s^{-1}, it is very likely that the source is unabsorbed.

3C 206 is a narrow-line, radio-loud QSO detected for the first time in hard X-rays (>20 keV). It was detected by Lawson & Turner (1997) using *Ginga* in the 2–10 keV The BAT spectrum is consistent with a pure power-law model with a photon index of $1.95^{+0.43}_{-0.39}$. 3C 206 was detected by the *ROSAT* PSPC with 0.37 counts s^{-1} during the all-sky survey (Voges et al. 1999); if we use the BAT power-law spectrum and extrapolate it to the 0.1–2.4 keV band, we find that no additional absorption (with respect to the Galactic one) is required to match the observed *ROSAT* count rate.

SWIFT J0844.9−3531 is a new hard X-ray source detected by Ajello et al. (2007). The BAT spectrum is consistent with a power-law model with a photon index of $1.91^{+0.46}_{-0.68}$. The flux in the 14–170 keV band is $1.7^{+1.1}_{-0.6} \times 10^{-11}$ ergs cm^{-2} s^{-1}. Rau et al. (2007) noted that this BXS source might likely be associated with the *ROSAT* source 1RXS J084521.7−353048.

SWIFT J0854.7+1502 is a new hard X-ray source detected by Ajello et al. (2007) and identified in Rau et al. (2007) as a Seyfert 2 galaxy. It has a flat spectrum which can be modeled as a power law with a photon index of $1.41^{+0.7}_{-0.9}$. A lower limit on the absorbing column density of 5×10^{21} atoms cm^{-2} can be derived by the nondetection of this source in the *ROSAT* all-sky survey.

SWIFT J0917.2−6221 is a new hard X-ray source. We analyzed a 7 ks XRT observation of this source. The XRT and BAT data are well fit by an absorbed power-law model with a photon index of $1.87^{+0.07}_{-0.04}$ and an absorbing column density of $1.33^{+0.18}_{-0.10} \times 10^{22}$ atoms cm^{-2}. A clear excess is present at energies <1 keV, and this can be well described as a blackbody component peaking at 0.14 keV. The flux and the luminosity in the 14–170 keV band are $2.6^{+0.8}_{-0.8} \times 10^{-11}$ ergs cm^{-2} s^{-1} and $20.0^{+6.0}_{-5.0} \times 10^{43}$ ergs s^{-1}.

Mrk 0704, or SWIFT 0918.5+1618, is another source found thanks to our algorithm (Ajello et al. 2007). During an XRT follow-up, the galaxy Mrk 704 was found as the BAT counterpart. Mrk 704 was previously detected in soft X-rays by *ROSAT* (Schwope et al. 2000). In a recent optical follow-up, the galaxy was found to be a Seyfert 1 (Masetti et al. 2006a). We have analyzed *ASCA*, XRT, and BAT data for this source. The best fit to the three data sets is a partial covering model in which the covering fraction is 0.5 and the power-law photon index is $1.36^{+0.10}_{-0.07}$. The source is highly absorbed, with a column density of $1.5^{+0.6}_{-0.3} \times 10^{23}$ atoms cm^{-2}. We also detected an iron line whose equivalent width is 160 eV.

4U 0919-54, detected at very high significance, is a LMXB also known to produce X-ray bursts (Jonker et al. 2001). Its spectrum is characterized by a steep photon index of 2.35 ± 0.25; alternatively, a bremsstrahlung model with a plasma temperature of $45.11^{+26.13}_{-9.80}$ keV yields a better χ^2.

MCG-01-24-012 is a Seyfert 2 galaxy already detected in hard X-rays by *BeppoSAX* (Malizia et al. 2002). When fitting both XRT and BAT data we find that the spectrum is consistent with an absorbed power law whose photon index is $1.7^{+0.08}_{-0.07}$ and intrinsic absorption is $6.5^{+0.8}_{-0.7} \times 10^{22}$ atoms cm^{-2}.

NGC 2992 is a Seyfert 1.9. The best fit for combined XRT, *ASCA*, and BAT data is an absorbed power law with a photon index of $1.24^{+0.06}_{-0.05}$ and an intrinsic hydrogen column density of $0.17^{-0.03}_{-0.03} \times 10^{22}$ atoms cm^{-2}. We also detected the presence of an unresolved Fe Kα line whose equivalent width is $0.52^{+1.0}_{-0.1}$ keV, in agreement with an old *BeppoSAX* measurement (Gilli et al. 2001) in which the reported column density is 1×10^{22} atoms cm^{-2}.

ESO 434-G040 is a known Seyfert 2 galaxy recently detected in hard X-rays also by *INTEGRAL* (Bird et al. 2006). A joint fit to *ASCA*, XRT, and BAT data with an absorbed power-law model yields a photon index of $1.77^{+0.006}_{-0.07}$ and a column density of $1.5^{+0.026}_{-0.09} \times 10^{22}$ atoms cm^{-2}. A clear excess below 2 keV can be modeled as a blackbody component with a temperature of $0.13^{+0.011}_{-0.016}$. An iron K_{α} line, with an equivalent width of 85.5^{+27}_{-33}, is also detected. The probability of the line being spurious is ~10^{-14}.

3C 227 is a Seyfert 1 galaxy and also a radio galaxy. The BAT spectrum is consistent with a power-law model with a photon index of $1.96^{+0.44}_{-0.58}$. This source was detected at a level of 0.016 counts s^{-1} in a 11 ks long *ROSAT* PSPC observation (0.1–2.4 keV; Crawford & Fabian 1995). In order to match the *ROSAT*-observed count rates, the extrapolation of the BAT power law to the 0.1–2.4 keV band requires an absorbing column density of at least 5×10^{21} atoms cm^{-2}. A recent *Chandra* observation confirms that 3C 227 is indeed an absorbed Seyfert 1. However, the joint *Chandra*-BAT spectrum is complex. Our best-fit model is the sum of an absorbed power-law

model and of a reflection component (both having the same photon index of $2.11^{+0.14}_{-0.24}$). The absorbing column density is $N_\mathrm{H} = 3.6^{+1.5}_{-1.4} \times 10^{22}$ atoms cm^{-2}. The reflection component seems to be large, $R > 1$, which is at odds with the absence of the iron K_α line. This source certainly deserves further investigations.

NGC 3081 is miscataloged in SIMBAD as a Seyfert 1 galaxy. In fact, the available 6dF spectrum shows clearly that this object is a Seyfert 2 object. We have analyzed *BeppoSAX* MECS and *ASCA* data for this source. The best fit is a sum of a blackbody component, peaking at $0.58^{+0.15}_{-0.11}$ keV, an absorbed power law with a column density of $60^{+3.1}_{-3.1} \times 10^{22}$ atoms cm^{-2} and a photon index of $1.9^{+0.02}_{-0.04}$, and an iron line with an equivalent width of 241^{+184}_{-131} eV.

REFERENCES

Ajello, M., Greiner, J., Kanbach, G., Rau, A., Strong, A. W., & Kennea, J. A. 2007, ApJ, submitted

Ajello, M., et al. 2006, Astron. Telegram, 697, 1

Antonucci, R. 1993, ARA&A, 31, 473

Arnaud, K. A. 1996, in ASP Conf. Ser. 101, Astronomical Data Analysis Software and Systems V, ed. G. H. Jacoby & J. Barnes (San Francisco: ASP), 17

Avni, Y., & Bahcall, J. N. 1980, ApJ, 235, 694

Barthelmy, S. D., et al. 2005, Space Sci. Rev., 120, 143

Bassani, L., Dadina, M., Maiolino, R., Salvati, M., Risaliti, G., della Ceca, R., Matt, G., & Zamorani, G. 1999, ApJS, 121, 473

Bazzano, A., et al. 2006, ApJ, 649, 9

Beckmann, V., Soldi, S., Shrader, C. R., Gehrels, N., & Produit, N. 2006, ApJ, 652, 126

Bird, A. J., et al. 2006, ApJ, 636, 765

Bolton, J. G., & Butler, P. W. 1975, Australian J. Phys. Astrophys. Suppl., 34, 33

Cappelluti, N., et al. 2007, ApJS, 172, 341

Comastri, A. 2004, in Supermassive Black Holes in the Distant Universe, ed. A. J. Barger (Dordrecht: Kluwer), 245

Comastri, A., Setti, G., Zamorani, G., & Hasinger, G. 1995, A&A, 296, 1

Crawford, C. S. & Fabian, A. C. 1995, MNRAS, 273, 827

Crawford, D. F., Jauncey, D. L., & Murdoch, H. S. 1970, ApJ, 162, 405

Deluit, S., & Courvoisier, T. J.-L. 2003, A&A, 399, 77

den Hartog, P. R., Hermsen, W., Kuiper, L. M., in't Zand, J. J. M., Winkler, C., & Domingo, A. 2004, Astron. Telegram, 261, 1

Donato, D., Sambruna, R. M., & Gliozzi, M. 2005, A&A, 433, 1163

Elvis, M., Plummer, D., Schachter, J., & Fabbiano, G. 1992, ApJS, 80, 257

Evans, I. N., Ford, H. C., Kinney, A. L., Antonucci, R. R. J., Armus, L., & Caganoff, S. 1991, ApJ, 369, L27

Fenimore, E. E., & Cannon, T. M. 1978, Appl. Opt., 17, 337

Gallo, L. C., Lehmann, I., Pietsch, W., Boller, T., Brinkmann, W., Friedrich, P., & Grupe, D. 2006, MNRAS, 365, 688

Gehrels, N., et al. 2004, ApJ, 611, 1005

Giacconi, R., Gursky, H., Paolini, F. R., & Rossi, B. B. 1962, Phys. Rev. Lett., 9, 439

Gilli, R., Comastri, A., & Hasinger, G. 2007, A&A, 463, 79

Gilli, R., Salvati, M., & Hasinger, G. 2001, A&A, 366, 407

Giommi, P., et al. 1991, ApJ, 378, 77

Götz, D., Mereghetti, S., Merlini, D., Sidoli, L., & Belloni, T. 2006, A&A, 448, 873

Gruber, D. E., Matteson, J. L., Peterson, L. E., & Jung, G. V. 1999, ApJ, 520, 124

Guainazzi, M., Matt, G., & Perola, G. C. 2005, A&A, 444, 119

Jonker, P. G., et al. 2001, ApJ, 553, 335

Landi, R., et al. 2007, ApJ, 669, 109

Laor, A. 2000, ApJ, 543, L111

Lawson & Turner 1997

Magdziarz, P., & Zdziarski, A. A. 1995, MNRAS, 273, 837

Malizia, A., Malaguti, G., Bassani, L., Cappi, M., Comastri, A., Di Cocco, G., Palazzi, E., & Vignali, C. 2002, A&A, 394, 801

Markwardt, C. B., Tueller, J., Skinner, G. K., Gehrels, N., Barthelmy, S. D., & Mushotzky, R. F. 2005, ApJ, 633, L77

Marshall, F. E., Boldt, E. A., Holt, S. S., Miller, R. B., Mushotzky, R. F., Rose, L. A., Rothschild, R. E., & Serlemitsos, P. J. 1980, ApJ, 235, 4

Masetti, N., Bassani, L., Dean, A. J., Ubertini, P., & Walter, R. 2006a, Astron. Telegram, 735, 1

Masetti, N., et al. 2006b, A&A, 459, 21

Matt, G., Guainazzi, M., & Maiolino, R. 2003, MNRAS, 342, 422

Matt, G., et al. 1997, A&A, 325, L13

McLure, R. J., & Jarvis, M. J. 2004, MNRAS, 353, L45

Merloni, A., Heinz, S., & di Matteo, T. 2003, MNRAS, 345, 1057

Metcalf, R. B. & Magliocchetti, M. 2006, MNRAS, 365, 101

Norton, A. J., Beardmore, A. P., Retter, A., & Buckley, D. A. H. 2000, MNRAS, 312, 362

Piccinotti, G., Mushotzky, R. F., Boldt, E. A., Holt, S. S., Marshall, F. E., Serlemitsos, P. J., & Shafer, R. A. 1982, ApJ, 253

Rau, A., Greiner, J., Salvato, M., & Ajello, M. 2007, A&A, submitted

Revnivtsev, M., Sazonov, S., Churazov, E., & Trudolyubov, S. 2006, A&A, 448, L49

Revnivtsev, M., Sazonov, S., Jahoda, K., & Gilfanov, M. 2004, A&A, 418, 927

Risaliti, G., Maiolino, R., & Salvati, M. 1999, ApJ, 522, 157

Sazonov, S., Revnivtsev, M., Krivonos, R., Churazov, E., & Sunyaev, R. 2007, A&A, 462, 57

Schmidt, M. 1968, ApJ, 151, 393

Schwope, A., et al. 2000, Astron. Nachr., 321, 1

Sikora, M., Stawarz, Ł., & Lasota, J.-P. 2007, ApJ, 658, 815

Slowikowska, A., Kanbach, G., Borkowski, J., & Becker, W. 2006, IAU, Joint Discussion 2, 8

Sowards-Emmerd, D., Romani, R. W., Michelson, P. F., & Ulvestad, J. S. 2004, ApJ, 609, 564

Treister, E., & Urry, C. M. 2005, ApJ, 630, 115

Tueller, J., et al. 2005, Astron. Telegram, 669, 1

Ueda, Y., Akiyama, M., Ohta, K., & Miyaji, T. 2003, ApJ, 598, 886

Voges, W., et al. 1999, A&A, 349, 389

Wheatley, P. J., Marsh, T. R., & Clarkson, W. 2006, Astron. Telegram, 765, 1

Worsley, M. A., et al. 2005, MNRAS, 357, 1281

Zamorani, G., et al. 1981, ApJ, 245, 357

Zdziarski, A. A., Poutanen, J., & Johnson, W. N. 2000, ApJ, 542, 703